CORA Cork Open Research Archive
Cartlann Taighde Oscailte Chorcaí

Title	Strategies for inorganic incorporation using neat block copolymer thin films for etch mask function and nanotechnological application
Authors	Cummins, Cian;Ghoshal, Tandra;Holmes, Justin D.;Morris, Michael A.
Publication date	2016-10-01
Original Citation	Cummins, C., Ghoshal, T., Holmes, J. D. and Morris, M. A. (2016) 'Strategies for Inorganic Incorporation using Neat Block Copolymer Thin Films for Etch Mask Function and Nanotechnological Application', Advanced Materials, 28(27), pp. 5586-5618. doi: 10.1002/adma.201503432
Type of publication	Article (peer-reviewed)
Link to publisher's version	https://onlinelibrary.wiley.com/doi/abs/10.1002/adma.201503432 - 10.1002/adma.201503432
Rights	© 2016 WILEY-VCH Verlag GmbH & Co. KGaA, Weinheim. This is the peer reviewed version of the following article: Cummins, C. , Ghoshal, T. , Holmes, J. D. and Morris, M. A. (2016), Strategies for Inorganic Incorporation using Neat Block Copolymer Thin Films for Etch Mask Function and Nanotechnological Application. Adv. Mater., 28: 5586-561, which has been published in final form at https://doi.org/10.1002/adma.201503432. This article may be used for non-commercial purposes in accordance with Wiley Terms and Conditions for Self-Archiving.
Download date	2026-10-31 12:42:05
Item downloaded from	https://hdl.handle.net/10468/6790



University College Cork, Ireland
Coláiste na hOllscoile Corcaigh

Strategies for inorganic incorporation using neat block copolymer thin films for etch mask function and nanotechnological application

Cian Cummins, Tandra Ghoshal, Justin D. Holmes, and Michael A. Morris *

C. Cummins, T. Ghoshal, M. A. Morris
Materials Research Group, Department of Chemistry and Tyndall National Institute, University College Cork, Cork, Ireland.
AMBER@CRANN, Trinity College Dublin, Dublin, Ireland.
*** Corresponding Author:** m.morris@ucc.ie

J. D. Holmes
Materials Chemistry and Analysis Group, Department of Chemistry and Tyndall National Institute, University College Cork, Cork, Ireland.
AMBER@CRANN, Trinity College Dublin, Dublin, Ireland.

Abstract

Block copolymer (BCP) nanolithography and their directed self-assembly (DSA) has emerged as a realizable complementary tool to aid optical patterning of device elements for future integrated circuit advancements. In this review, methods to enhance BCP etch contrast for DSA application and further potential applications of inorganic nanomaterial features (*e.g.* semiconductor, dielectric, metal and metal oxide) are examined. Strategies to modify, infiltrate and controllably deposit inorganic materials by utilizing neat self-assembled BCP thin films open a rich design space to fabricate functional features in the nanoscale regime. This review provides the reader with an understanding and overview on innovative ways for the selective inclusion/infiltration or deposition of inorganic moieties in microphase separated BCP nanopatterns. Early initial inclusion methods in the field and exciting contemporary reports to further augment etch contrast in BCPs for pattern transfer application are described. Specifically, the use of evaporation and sputtering methods, atomic layer deposition, sequential

infiltration synthesis, metal-salt inclusion and aqueous metal reduction methodologies forming isolated nanofeatures are highlighted in di-BCP systems. Functionalities and newly reported uses for electronic and non-electronic technologies based on the inherent properties of incorporated inorganic nanostructures using di-BCP templates are highlighted. We also outline the potential for extension of incorporation methods to triblock copolymer features for more diverse applications. Lastly, challenges and emerging areas of interest for inorganic infiltration of BCPs are discussed.

Keywords: Block copolymers, infiltration and incorporation, metals, etch contrast, inorganic nanomaterials.

1. Block copolymers

Self-assembly (SA) is a reversible process whereby pre-existing disordered components form a highly ordered arrangement or pattern under the right conditions. It should be noted that there are two main types of SA; dynamic and static. Static SA involves systems that do not dissipate energy and are at local equilibrium. In contrast, dynamic SA (also referred to as self-organisation) may require energy for an ordered structure to form. This reversible spontaneous process of SA is summarised from the Gibbs Free Energy equation below; [1]

$$\Delta G_{SA} = \Delta H_{SA} - T\Delta S_{SA} \qquad \text{Equation 1}$$

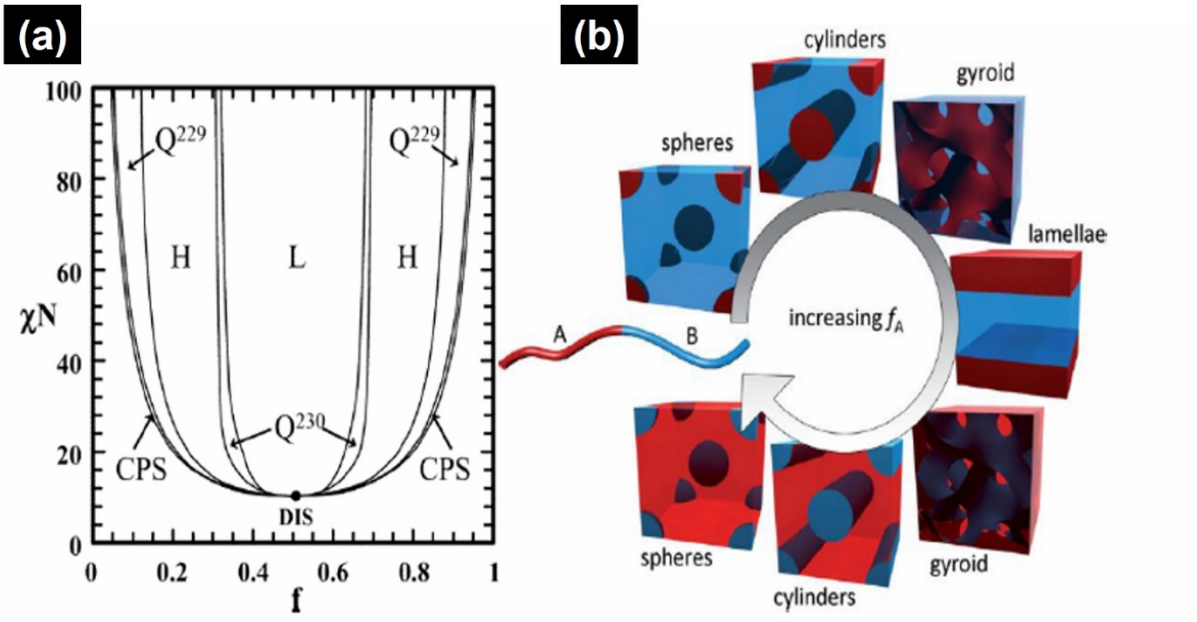
ΔG_{SA} when negative self-assembly is a spontaneous process

ΔH_{SA} enthalphy change due to interaction between segments of BCP

$T\Delta S_{SA}$ entropy change in process

From equation 1 we can conclude that for a given system above a certain temperature for SA to occur, the enthalpy term must be negative and in excess of the entropy term. Thus for SA to successfully occur, enthalpic forces must dominate.

A large number of reviews are available on block polymer (BCP) synthesis,[2],[3],[4] thin film behavior and morphologies for nanopatterning,[5],[6],[7],[8],[9],[10],[11],[12],[13],[14],[15],[16],[17],[18],[19] and thus only the fundamental influencing parameters concerning the nanopattern formation of BCPs are detailed here. The simplest form of a BCP is one that contains two polymer blocks covalently connected at their ends *i.e.* a diblock copolymer (di-BCP) as shown in **Figure 1**.[20]



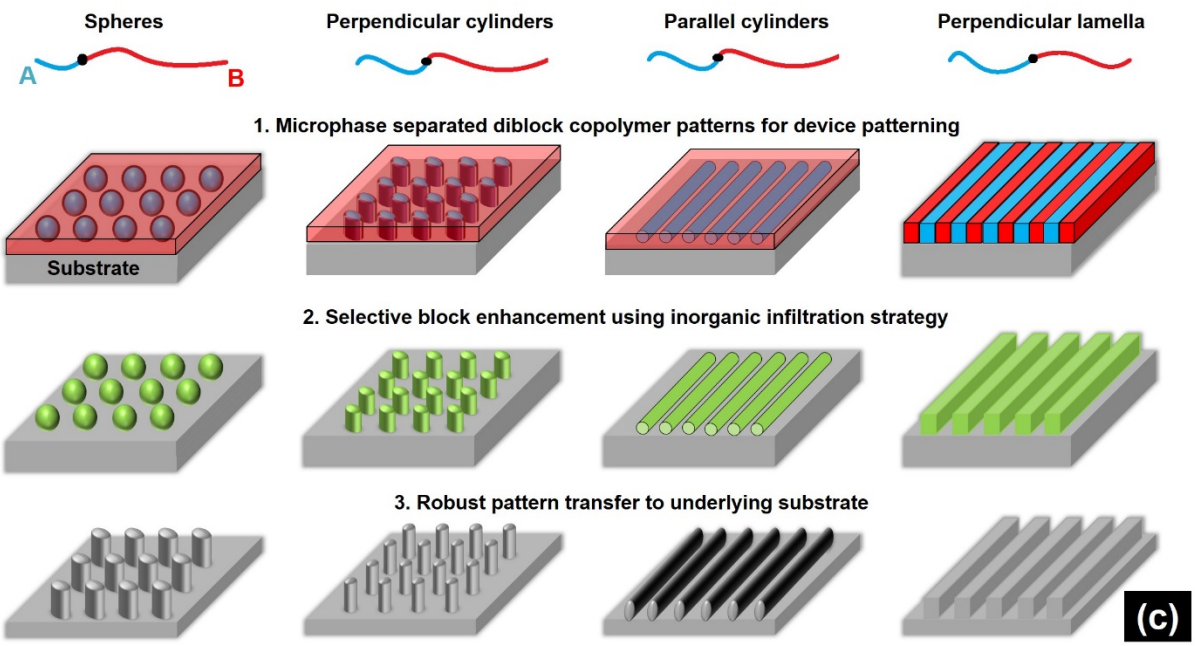


Figure 1. (a) Phase diagram of a diblock copolymer with volume fraction vs χN as predicted by self-consistent mean field theory. (b) Resulting morphologies on increasing block volume fraction (f_A). See text for details. (c) Schematic representing paths to well-defined high aspect ratio features using di-BCP systems and infiltration techniques. 1. Successful self-assembly of di-BCP system forming ordered arrays. 2. Selective incorporation of one block with inorganic material to enhance etch contrast. Inorganic features at substrate surfaces can also be utilized for other functions (see text for details). 3. Pattern transfer using inorganic etch masks.

Table 1. Corresponding block percentages and space groups for resulting morphologies of "classical" block copolymers.[21]

Morphology	**Space Group**	**Percentage of block A**
Spheres	lm3m	0-21%
Cylinders	p6mm	21-33%
Double Gyroid	la3d	33-37%
Double Diamond	pn3m	33-37%
Lamallae	Pm	37%-50%

The block volume fractions (f_A and f_B, where $f_A + f_B = 1$) and the polymer-polymer interaction parameter (referred to as the chi factor, Flory-Huggins χ_{AB} parameter or simply χ) contribute to resulting morphology and the self-assembly dynamics of di-BCP materials.[22] The χ value quantifies the degree of dissimilarity of constituent chains. Di-BCPs have properties that can be utilized for diverse functions which are not accessible from their homopolymer segments.

Upon "nanophase separation", more commonly referred to as microphase separation, di-BCPs can form well-defined nanoscale spherical, cylindrical, gyrodial or lamellar features (see Table 1 and Figure 1a) with increasing *f* as shown in Figure 1b. The thermodynamic incompatibility (unfavourable interactions) of the constituent polymer segments is the driving force for microphase separation. Di-BCPs (A-B) form geometries that can be tuned or where one can "dial-in" specific nanoscale dimensions (3-100 nm) via control of the total degree of polymerization ($N = N_a + N_b$).[16]

These factors are represented by equation 2 which describes the free energy of the system:[23]

$$\frac{\Delta Gmix}{KbT} = \frac{1}{NA}\ln(f_A) + \frac{1}{NB}\ln(f_B) + f_A f_B \chi \qquad \text{Equation 2}$$

Where $\Delta Gmix$ = Gibbs free energy, K_b = Boltzmann's constant, T = Temperature, N_A = Polymerization of segment A, N_B = Polymerization of segment B, f_A = Volume fraction of block A, f_B = Volume fraction of block B, and χ = Flory-Huggins Interaction Parameter

From equation 2, terms 1 and 2 are determined by the degree of polymerization of the BCP and relative volume fractions. In contrast term 3, χ, is a result of the molecules involved (f_A and

f_B) and is directly related to temperature. The phase diagram displayed in Figure 1a shows the relationship of χN versus f. If χ and/or N value are reduced so that χN is below a critical value, entropic factors will produce a disordered phase. It should be noted that χN plays a pivotal role in microphase separation occurring and theoretically a χN value above ~ 10.5 is needed for ordered morphologies to occur. χ is determined by the di-BCP chosen while the volume fraction and polymerization which influence the translational and configurational entropy are determined by the polymerization stoichiometry. As determined from equation 2, χ is a temperature dependent parameter. For an ordered structure at equilibrium, polymer chains of the di-BCP will be arranged in minimum free energy configurations.

2. Motivation and scope

The empirical law known as "Moore's Law" drives the nanoelectronic industry to continually achieve ever smaller technology nodes for increased electronic device performance.[24] Due to physical limits and prohibitive costs encountered with optical lithography patterning, alternative methodologies are being investigated and scrutinized. Additionally, major semiconductor companies also face challenges to evolve and diversify devices (More than Moore, MtM), together with advanced connectivity (Internet of Things, IOT). It has been reported extensively in recent years that block copolymer (BCP) self-assembly may be promising enough to afford the nanoelectronic industry an alternative patterning technology.[25],[26],[27],[28],[29] Highly ordered BCP etch mask arrays with near perfect registration could possibly augment next-generation lithographic processes so as to move industrial scale patterning into the deep nanoscale regime (sub-10 nm) while reducing costs and maintaining throughput for high volume manufacturing (HVM) needs.

Research on BCP materials, enhancing polymer block etch contrast, reducing line edge/width roughness, minimizing defect levels, high-aspect ratio pattern transfer and overall integration for electronic device patterning is being relentlessly developed in pursuit of Moore's Law,[30] a trend followed for continued silicon feature miniaturization over the past 50 years. Top-down optical patterning of substrates to fabricate trenches (graphoepitaxy, hard[31] or soft[32]) and chemically modify polymer interactions at random copolymer brush coated substrate surfaces (chemoepitaxy[33],[34]) to "direct" self-assembly are referred to as directed self-assembly (DSA) of BCPs. DSA of BCPs coupling top-down fabrication with BCP self-assembly provides a powerful synergy to fabricate device related geometries with the potential to further increased demands of microprocessor and hard disk drive companies.[35] The benefit of DSA of BCPs lies in the technology's conceptual similarities and parallel processing schemes (see Figure 1c for BCP patterning and infiltration process) to current device patterning where a light sensitive polymeric based layer (photoresist) is spun on a substrate and is patterned with ultraviolet light to attain device relevant features (*e.g.* line, holes). These patterned resist features are subsequently "pattern transferred" to the underlying material.

There are still outstanding issues with BCP nanolithography patterning for HVM and very large scale integration (VLSI). One major concern is the poor etch contrast between polymer blocks to enable high fidelity device structures following pattern transfer.[36] In general, improving etch contrast or etch resistance can be achieved by incorporating metallic based moieties as these are chemically resistant to oxygen plasma processes employed to remove polymeric carbon species, which generally constitute the majority framework of BCPs. One must also consider the pattern transfer process and gases used to etch or remove the underlying substrate relative to the infiltrated etch resistant material. The hardmask or etch stop must be fabricated with consideration for the gases involved to avoid its' elimination or removal and thus retain

its' physical integrity so that the underlying substrate can still be etched at a high rate to create high fidelity features upon pattern transfer (see Figure 1c). Thus, infiltrating self-assembled BCP nanopatterns with inorganic moieties to chemically enhance the etch resistance of the pattern is extremely useful. Since most BCP systems are made up primarily of lighter elements (*e.g.* C, H, O, N) and thus have poor etch contrast, incorporating heavier metal containing species has great potential for etch enhancement. As-synthesized metal containing BCPs have been highlighted recently to circumvent this issue and two reviews are available.[37],[38] Therefore, this review aims to provide an overview of versatile ex-situ infiltration techniques on as-formed BCP patterns. Ideally, BCP materials should allow a facile highly selective pattern transfer resulting in high aspect ratio features (*i.e.* the ratio of lateral to vertical dimensions) as shown in Figure 1c.

The potential of infiltration of "neat" BCPs was outlined in 2006 by Krishnamoorthy *et al.*[10], "*In addition to in-situ synthesis of nanoparticles, block-copolymer-derived templates can be used to assemble "preformed" nanoparticles into a variety of ordered arrangements*". This statement referred to only a handful of early demonstrations as we will discuss below. However, at present a diverse range of techniques have been established for superb control of directing nanoparticles and inorganic material using neat di-BCPs. There are a number of reasons why such post BCP self-assembly modifications are advantageous for on-chip etch masks. Firstly, achieving well-defined inorganic nanostructures post self-assembly avoids complexities that can alter kinetic and thermodynamic paths when bonding materials (*e.g.* metal salts, small molecules) with BCPs in solution.[39] Furthermore, the range of BCP materials in solution that can be selectively altered is quite narrow (restricted to electron donating sites in BCP blocks like poly(2-vinylpyridine) (P2VP) and poly(4-vinylpyridine) (P4VP), or weakly coordinated with poly(ethlylene oxide) (PEO) blocks). Consequently, it is

difficult to produce well-oriented and ordered microphase separated BCP patterns of technological use with high registration and global coverage. Lastly, morphological changes are also a concerning factor when adding materials in solution that may result in atypical BCP structures following thin film preparation. In this respect, the surface energetics at the polymer/substrate and free interface (polymer/air) must be given special attention for BCP thin films to self-assemble with desired orientation and lateral ordering with appropriate treatment techniques. Two popular annealing methods for inducing self-assembly and enhancing the long range order of BCPs are solvent vapor annealing[40] and thermal annealing.[13],[41] These two annealing methods would presumably behave differently in comparison to accepted annealing protocols for forming thermodynamically stable structures when materials are bonded in solution due to changes including but are not limited to BCP volume fraction, glass-transition temperature, crystallinity, polymer chain mobility, block surface energies and free air/polymer and polymer/substrate interface interactions. Other methods for inducing microphase separation and long range BCP order that could potentially behave in an adverse manner include solvothermal annealing,[42],[43] shear alignment,[44] microwave annealing,[45] and the recently developed immersion annealing[46]. Readers should note that the infiltration methods detailed herein avoid perturbation of the neat BCP films, *i.e.* morphological changes have not been reported following infiltration of the self-assembled structure, and such routes represent excellent strategies for post self-assembly inorganic nanofeature fabrication.

Strategies for enhancing and infiltrating a particular polymer block component have been demonstrated across a range of BCP systems. Beyond on-chip etch mask applications for nanolithography, the alterations to BCP systems enable the formation of hybrid nanoscale materials with novel functionalities and salient work is described in sections below. Through selective infiltration of “foreign” species within selective BCP microdomains, resulting

nanostructures can potentially address a range of electronic, environmental and energy applications in low-cost scalable processes. Although this review focuses on di-BCP structures, other linear BCP structures such as triblock polymers (ABA, ABC) and multiblock polymers [(AB)n] can access a myriad of zero, one, two, and three dimensional architectures increasing design space for future materials and could possibly be infiltrated in the same manner as di-BCP copolymers. We comment on triblock polymer materials in the penultimate section of this review to provide further insights into potential future directions. In a recent research news article, Ross *et al.*[47] emphasized the potential of utilizing 3D BCP patterns for batteries, membranes or photovoltaic application as placement of features and defect levels are not as stringent as for integrated circuit application. With this in mind, the ability to replicate 3D BCP patterns using inorganic strategies described in this review may allow low-cost high density fabrication practices for nanomanufacturing.

The following reports and analysis on incorporation methods for BCP films detailed in this review can generally be classified as either an “additive” or “subtractive” lithographic process. An additive process typically involves the evaporation or sputtering of material into a porous template (conventionally referred to as a resist layer in semiconductor lithographic manufacturing for micro/nanofabrication) to pattern features at the substrate surface and the template is then subsequently removed, *i.e.* lifted off. One major issue concerning additive processes is the lift-off procedure, as uniformity can be problematical at small dimensions. In contrast, a subtractive process usually entails a uniform layer being grown or deposited followed by the application of a template or resist layer. The process then involves etching (wet or plasma) the exposed underlying layer while the template protects the area to be patterned.[48] Concerns for such practices centre on attaining large area feature uniformity through avoiding film undercut or sidewall profile variations and thus optimizing wet etching or plasma etching

to retain feature integrity. Below, we examine reports based on BCP templates utilizing such additive and subtractive processes as well as innovative variations that avoid complex parameter issues in order to yield regularly defined inorganic features for nano-applications.

Specifically, we examine emerging methodologies developed over the past decade for insertion of inorganics in BCP templates and are as follows; (i) evaporation and sputtering of metals on BCP templates; (ii) atomic layer deposition (ALD) methods and BCP templates; (iii) sequential infiltration synthesis (SIS) of BCPs; (iv) spin coating methodologies for metal nanoparticle alignment and metal oxide inclusion with "activated" BCP templates, and (v) aqueous metal reduction (AMR) and BCP nanopatterns. Each section describes reports on as-formed (*i.e.* "neat") BCP patterns for their etch mask and functional use. In reviewing the different methodologies for fabricating inorganic material, we also highlight the specific BCP system attributes within sections that allow facile infiltration due to their inherent chemical properties to form porous templates or their reactivity for chemical reactions with precursor material.

3. Inorganic incorporation methodologies for "neat" diblock copolymer patterns

3.1. Evaporation and sputtering of metals on block copolymer templates

Over a decade ago, Park *et al.*[49] demonstrated a high level of control to fabricate hexagonally packed metal dot arrays with an areal density of 10^{11} cm^{-2}. A cylinder forming poly(styrene)-*block*-poly(isoprene) (PS-*b*-PI) BCP was employed to form large scale coverage of nanodot patterns to behave as an etch mask. A trilayer pattern-transfer scheme was utilized, consisting of a top layer of BCP, a middle layer of silicon nitride and a bottom layer of polyimide, as shown in **Figure 2**. The authors described that the trilayer pattern transfer route was adopted in order to increase the aspect ratio of pattern transferred features as previous work displayed an aspect ratio of ~ 1.[50] Their previous work in 1997 reported the first demonstration of pattern

transfer with a BCP, using a sphere forming PS-*b*-poly(butadiene) (PS-*b*-PB) BCP. Two years prior to this experimental pattern transfer evidence, the original concept for adopting BCP films as etch masks for patterning small features was formulated by Mansky *et al.*[51],[52]

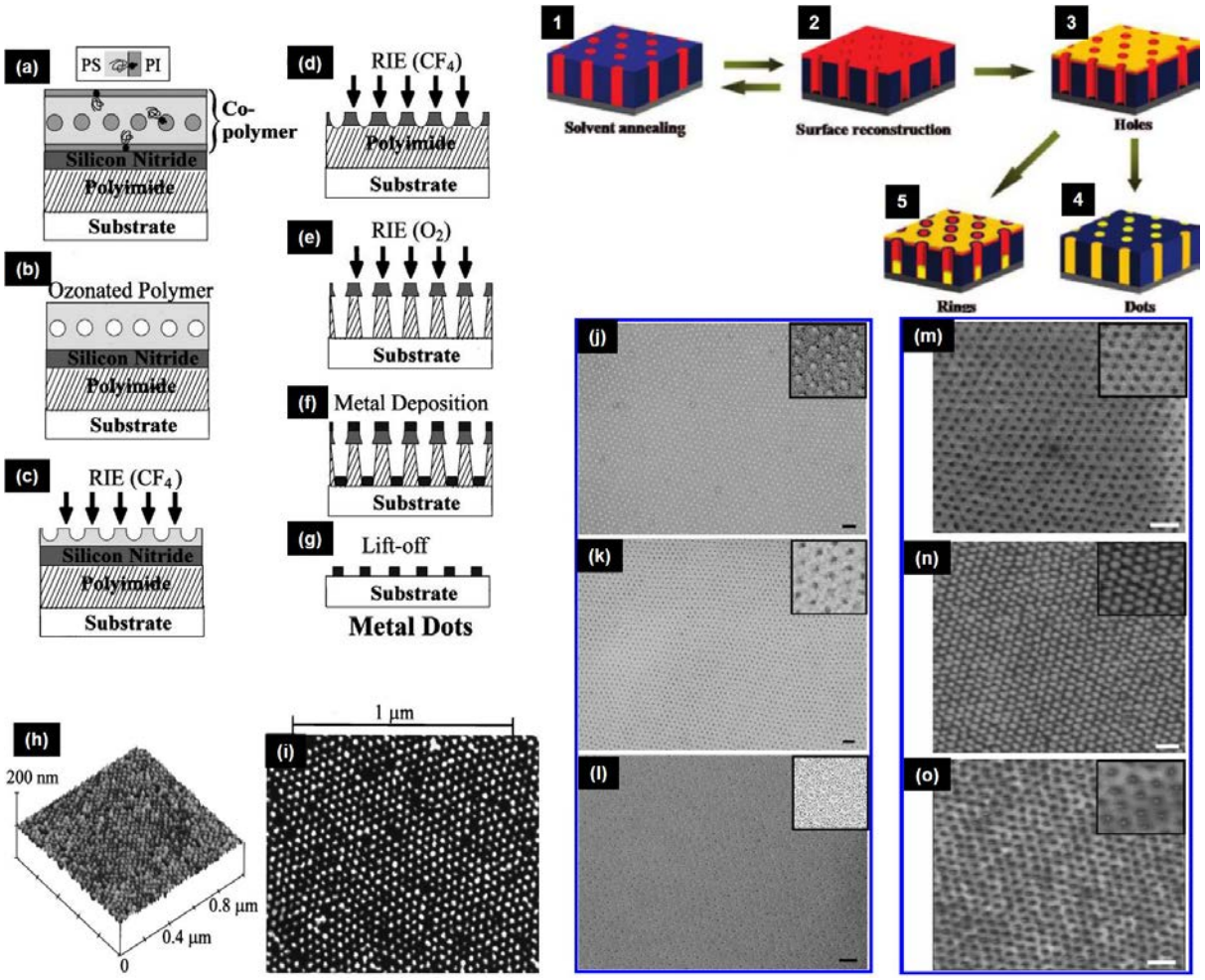


Figure 2. a-g) Process flow of trilayer pattern transfer strategy using PS-*b*-PI for templating Au nanodots via lift-off. h and i). AFM and SEM images of Au nanodots with an areal density of 10^{11} cm^{-2}. 1-5) Process flow for Au decoration on "surface reconstructed" PS-*b*-P4VP films. j-o) TEM images of Au decoration via glancing angle evaporation (~ 5°) on surface reconstructed PS-*b*-P4VP films j) Au outside the P4VP pore after evaporation, k) inside the P4VP pore using <0.5 nm Au layer through thermal annealing at 115°C for 10 minutes, and l) having a ring pattern using a Au layer > 0.5 nm thermally annealed 180 °C for 30 minutes. m-

o) SEM images following reactive ion etching of etch masks into underlying silicon oxide generating m) pores, n) pillars, and o) ring patterns. All scale bars = 100 nm.

These initial works outlined the requirement for careful attention to BCP selection and chemistry for on-chip etch-mask application. As reported by Park *et al.*, the minor PI block of PS-*b*-PI BCP was removed via ozonolysis and washing of fragments as the carbon-carbon double bond backbone of the PI block is susceptible to fragmentation (similar to the PB block in PS-*b*-PB[50],[52]) enabling a porous PS matrix to be formed (Figure 2c). Subsequent RIE processes developed a porous polyimide pattern (Figure 2e). Consecutive evaporation processes of Ti and Au (5 nm/15 nm) were used to in-fill the porous polyimide area (Figure 2f). Following lift-off of the polyimide material, well-ordered Au nanodots were fabricated (Figure 2h and i).

The above mentioned successes showed the capabilities of BCPs to form well-defined on-chip nanopatterned etch masks for pattern transfer into the underlying substrate but, more importantly, demonstrated a relatively simple process route to allow placement and registration of metal arrays in the sub-20 nm diameter regime. Following Park *et al.*'s work, further studies using evaporation of metallic material on neat BCP films largely concerned with PS-*b*-poly(methyl methacrylate) (PS-*b*-PMMA). One such report[53] used a porous PS-*b*-PMMA template where PMMA was selectively removed through UV exposure (and acetic washing) as PMMA is susceptible to scission. Interestingly, with the PS etch mask in place on silicon, an underlying silicon electrode of a metal oxide semiconductor capacitor was roughened via dry etching thus increasing device surface area.[54] Additionally, porous PS templates were employed to demonstrate highly ordered Au, Co and Ti nanodot arrays after e-beam evaporation and removal of the PS material.

The earliest works on modification and infiltrating PS-*b*-PMMA BCPs as described[53],[54] centred on thermal or e-beam evaporation of metals combined with lift-off procedures. Another example presented by Russell and co-workers[55] using PS-*b*-PMMA templates and Cr evaporation in 2002 demonstrated a similar level of areal density (10^{11} cm^{-2}) to Park's[49] work. PMMA was initially removed via the UV exposure/acetic acid washing protocol generating a porous matrix. Note that PMMA removal via dry plasma etching is well understood and can be etched completely using a controlled combination of trifluromethane and oxygen gases.[56],[57] Metal evaporation allowed Cr nanodots to be formed after PS matrix removal. Interestingly, the authors also reported on the fabrication of a Cr matrix via an inverse PS-*b*-PMMA system (*i.e.* f_{PMMA} = 0.7, PMMA matrix surrounded by PS dots). After selectively removing the PMMA matrix, Cr evaporation (15 nm) enabled a porous Cr matrix to be generated following excess PS and Cr elimination. The work extended the use of BCP templates to act as both negative and positive templates. Succeeding publications on PMMA based etching and lift-off methods have demonstrated graphoepitaxially aligned magnetic Co nanodots using a dry lift-off procedure,[58] fabrication of high-aspect ratio (1:10) Si nanopillars using sputtered Cr,[59] high temperature resistant Au nanoparticles,[60] ultra-small ferromagnetic (Co) nanorings,[61] Ag nanowires (also fabricated via electrochemical etching),[62] selective masked deposition of Fe catalyst particles for carbon nanotube growth,[63] Au and Al nanowire arrays guided by soft graphoepitaxy,[64, 65] Al_2O_3 dot nanopatterning on Cu substrates,[66] silicon nanocrystals,[67] and Ge nanowire fabrication.[68] Whilst generally not widely employed, one should note that electrodeposition methods have also been used to deposit inorganic material in porous PS-*b*-PMMA films as demonstrated in excellent work by Thurn-Albrecht *et al*.[69] In relation to evaporation methods, a report in 2007 attempted to selectively decorate evaporated Ag on electron-beam lithographically exposed PS-*b*-PMMA

BCPs. The authors observed less Ag decoration in electron-beam exposed areas and commented how the methodology could potentially be utilized to tailor a BCP system domain selectivity where an inherent attraction is not present.[70] In 2014, Kreuzer *et al*.[71] outlined an unusual phenomenon whereby either mesoporous Ti films were formed on a low molecular weight unmodified PS-*b*-PEO template (period of dots ~ 40 nm) or hexagonally arranged Ti dots were formed on a larger molecular weight template (period of dots ~ 100 nm) after electron-beam evaporation of a nominal 10 nm of Ti. The report showed that by choosing a particular template different meso or nano structures could be formed. The work also emphasized that surface chemistry is not the sole dominating factor for selective evaporation and the dimensions of features of a template must also be considered.

One work highlighting the elegance and versatility of BCP materials using PS-*b*-poly(4vinyl-pyridine) (PS-*b*-P4VP) demonstrated pattern transfer of pores, pillars and rings into silicon oxide via gold evaporated etch masks on a PS-*b*-P4VP template as shown in Figure 2.[72] The PS-*b*-PxVP (x = 2 or 4) systems have received much study owing to the reactive PVP groups for metal or small molecule bonding and their inherently high χ (PS-*b*-P2VP, χ ~ 0.18). The authors took advantage of selective solvent swelling of P4VP to create a "surface reconstructed" or porous film. Glancing angle gold evaporation along with thermal annealing enabled the formation of different Au patterns, *i.e.* depending on thermal annealing temperature and time, Au nanoparticles or rings could be attained due to differing P4VP-Au interactions as shown in Figure 2j-l. The patterns were subsequently used as etch masks to etch into the SiO_2 underlayer (Figure 2m-o).

The first demonstration of a metal nanodot memory array using a BCP lift-off technique was reported by Hong *et al*.[73] in 2010. Porous PS-*b*-PMMA nanodot patterns were utilized for Cr

nanodot fabrication via evaporation and lift-off of the PS template. Subsequent ALD coating of a control oxide (Al_2O_3) on the Cr nanodots and an evaporated metal gate (Ti/Al layers) were carried out to fabricate the memory device (See **Figure 3**h-i). The authors reported an "*ultrawide memory window*" (15 V) for their device. Importantly, it was concluded that the density of the device features could certainly be extended beyond the 40 nm period of Cr dots used by the range of "*other copolymer systems with stronger segregation forces*". This statement is certainly true from examining today's BCP processes where nanodot templates with periods of 18 nm,[74] 17 nm,[75],[76] 12 nm,[77],[78] and 10 nm[79] have been fabricated with high χ BCP materials.

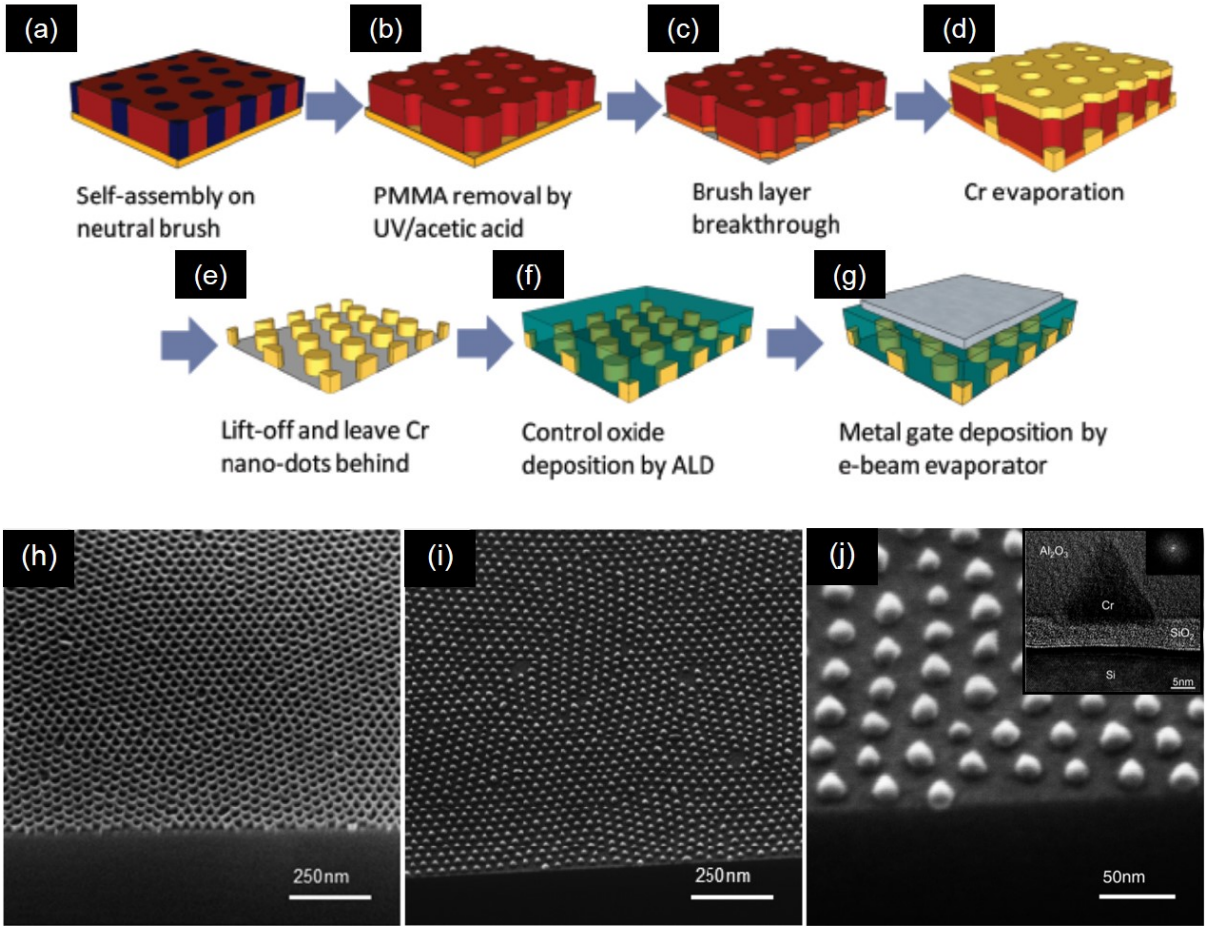


Figure 3. a-g) Process flow for metal nanodot memory device using PS-*b*-PMMA and Cr evaporation. h) Side-view SEM image of porous PS matrix following selective PMMA

removal. Top-down i) and side-view j) SEM images of evaporated Cr nanoarrays using host PS matrix. Inset in j) shows TEM image of gate oxide on Cr dot.

An interesting demonstration by Kim *et al.*[80] in 2015 described the use of BCP nanopatterning for triboelectric generator application. Triboelectric nanogenerators have gained interest for energy harvesting and BCP patterning has been proposed due to the associated low device fabrication costs. In Kim's work, PS-*b*-PMMA was spin coated on a Au coated Kapton film producing an arrangement of vertically oriented PMMA cylinders (**Figure 4**) in the PS matrix. Successful thermal evaporation of Au into the porous PS template (via UV/acetic acid protocol) and subsequent lift-off of the PS matrix produced high density Au nanodots. After device fabrication using the Au nanodots from BCP patterning, current output of the triboelectric nanogenerator increased at least 16 times. An earlier work by Jeong *et al.*[81] also demonstrated triboelectric nanogenerator devices via different SiO_2 patterns (nanodots, nanogrates, and nanomeshes) from a PS-*b*-PDMS BCP. SiO_2 nanomesh features proved to be the best performing morphology and is a key consideration to further aid efforts in the future for achieving high-performance triboelectric nanogenerators. While Jeong's work was based on a BCP containing an inorganic moiety (PDMS), enhanced future device performance could be achieved by pursuing more diverse inorganic material inclusion as demonstrated in Kim's work. As alluded to in the introductory section, such etch resistant patterns can also be directly formed from BCPs containing metal or silicon blocks, *e.g.* poly(ferrocenylsilane) and poly(dimethylsiloxane). After brief oxygen etching of such self-assembled films to remove a susceptible carbon based block; holes, pillars, *etc.* can be created as an on-chip etch masks. Such alluring systems offer a viable route for functional use as described above[81]. Furthermore, SiOx patterns generated from PS-*b*-PDMS films have been used as etch masks to pattern poly(3,4-ethylenedioxythiophene):poly(styrenesulfonate) to behave as an ethanol

vapor sensor[82], for resistive memory application on graphene and metal electrodes[83], and for graphene quantum dot fabrication[84].

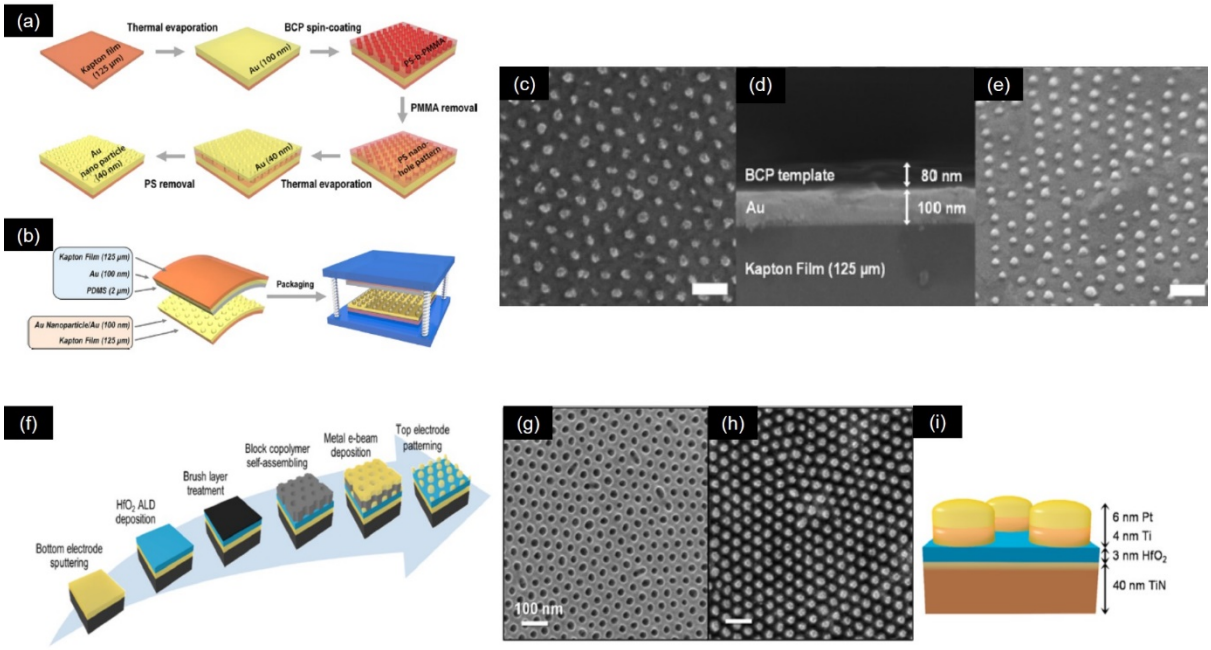


Figure 4. a and b) show process flow for triboelectric nanogenerators. c-e) Top-down SEM and side-view SEM of Au nanodots following evaporation for triboelectric device. f) Process flow for development of bilayer Pt/Ti nanodots on HfO_2/TiN surface for resistive switching memory application. Top-down SEM image of g) porous host PS template and h) Pt/Ti nanodots as shown schematically in i). All scale bars = 100 nm.

Others have also lately reported device fabrication for memory application using PS-*b*-PMMA templates. Frascaroli *et al.*[85] developed resistive switching in a high-density device using bilayer Pt/Ti nanodots at a density of 5 x 10^{10} devices cm^{-2}. The work highlights the ability of BCPs to address HVM needs where scalability and high device density are necessary, which can be difficult to access with expensive top-down patterning methods alone. Note that the bilayer of Pt/Ti nanodots were patterned on a HfO_2/TiN surface (see Figure 4f-i) and electrically characterized using a conductive atomic force microscope.

Many studies have been published combining BCP dot templates and evaporated metal with a focus on magnetic studies. One-dimensional metal nanowires are also of interest for a plethora of diverse functions including optoelectronic, photonic and solar-cell devices. The above outlined approaches using evaporation and BCP templating generally involve a lift-off procedure. In contrast, excellent work has been shown by Ross and co-workers using PS-*b*-poly(dimethyl siloxane) (PS-*b*-PDMS) templates and radio frequency sputtering of a variety of metals coupled with plasma etching.[86],[87],[88],[89] PS-*b*-PDMS is a BCP of major focus in the BCP nanopatterning community due to its high χ ($\chi \sim 0.26$) and the PDMS block is a silicon containing backbone producing etch contrast when oxidized. After developing well-oriented oxidized PDMS line-space features following selective etching, radio frequency sputtering of Ti, W, Pt, Co, Ni, Ta, Au and Al along with selective dry etching of the sputtered metal led to resulting metal wires with sub-10 nm feature size.[86] **Figure 5**a displays SEM data of the respective metals fabricated using this "Damascene-like" process with periods of 17 nm. Importantly, the fabrication process was shown to be robust as studies revealed that the Ni nanowires retained their magnetic properties. A previous article reported the use of a cylinder forming PS-*b*-PDMS system directed via graphoepitaxy along with radio frequency sputtering of Co to form impressive ferromagnetic concentric double ring patterns.[88] Another work detailed a similarly impressive level of control in generating nanopore arrays via a sphere forming PS-*b*-PDMS template and radio frequency sputtering of metals for magnetic study (Figure 5b-i).[89]

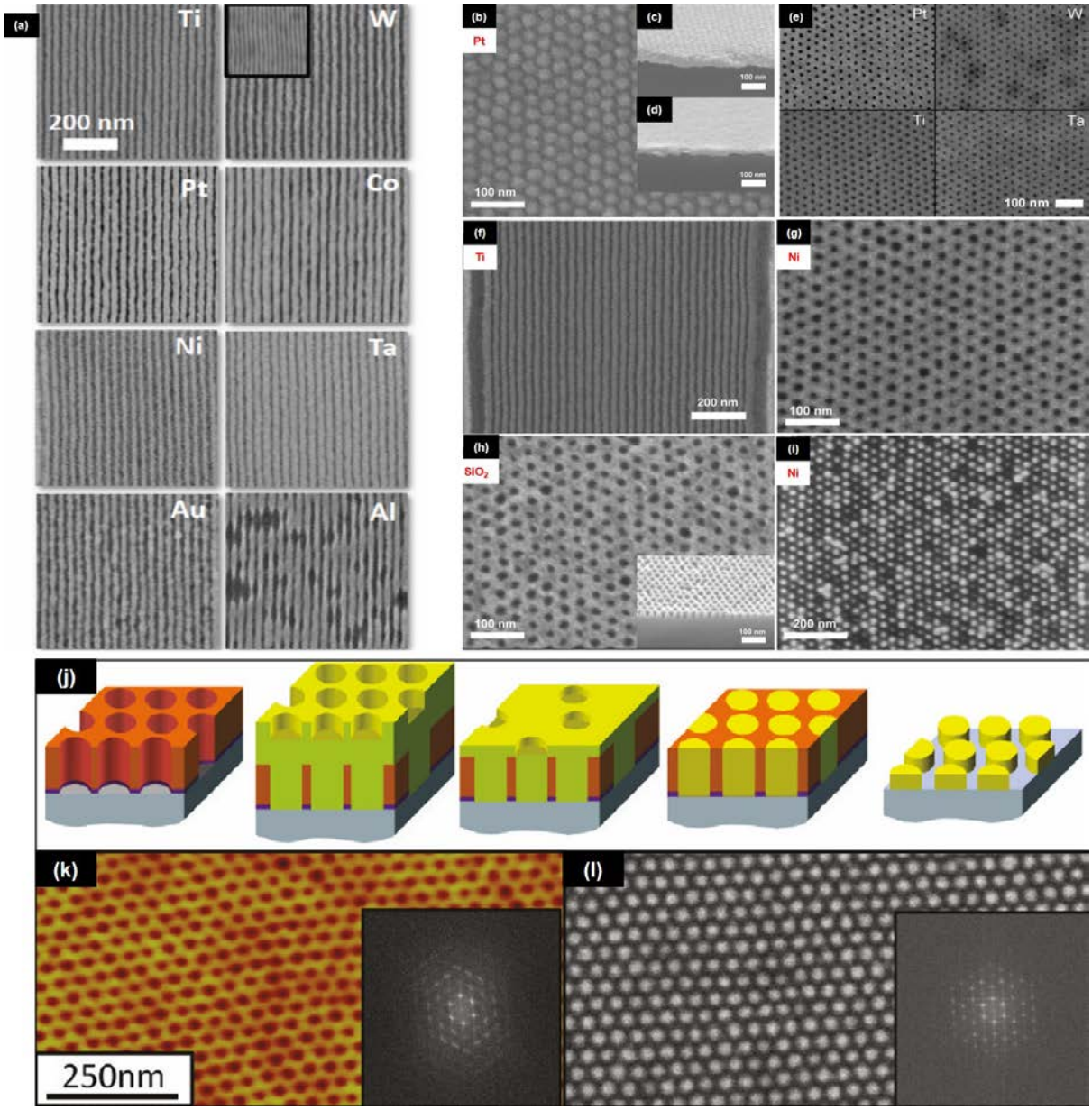


Figure 5. a) Top-down SEM images of diverse metallic lines fabricated from robust process using PS-*b*-PDMS templates and metal radio frequency sputtering. b) Pt deposited on PDMS spheres. e) Metallic porous films after selective PDMS removal, f) Ti lines, g) a nanoporous Ni metallic film, h) porous SiO_2 following etching using nanoporous metallic film, and i) Ni nanodots. j) "Damascene-like" process for the generation of permalloy nanodots using PS-*b*-PLA BCP. k) Porous PS matrix after PLA etching. l) SEM image of highly ordered permalloy nanodots fabricated using molecular beam deposition followed Ar ion beam milling.

More recently, Baruth *et al.* also described a “Damascene-like” process by overfilling a porous PS template generated from a cylinder forming PS-*b*-PLA BCP (Figure 5j and k).[90] After overfilling $Ni_{80}Fe_{20}$ (permalloy) through molecular beam deposition, planarization using ion beam milling to the PS matrix followed by dry etching enabled the formation of $Ni_{80}Fe_{20}$ nanodots as shown in Figure 5l. The authors also described a climate controlled process enhancing the ordering PS-*b*-PLA features during self-assembly. A considerable difference in the long range order of the BCP was observed between the two studied annealing environments and thus the resulting evaporated patterned $Ni_{80}Fe_{20}$ material. Of late, further work on the PS-*b*-PLA system has led to even greater control in the degree of order and the resultant incorporated metal material.[74]

The opening part of section 3.1 provided an overview of early research of metal incorporation via evaporation (thermal, e-beam) and sputtering using BCP templates as hosts that has catalysed more incorporation techniques to be investigated and led to further achievements. Latterly the work has progressed to achieve finer definition and registration of metals via graphoepitaxial alignment. These last-mentioned works attaining high-quality ordered patterns can partly be attributed to the use of high χ (*e.g.* PS-*b*-P4VP, PS-*b*-PDMS and PS-*b*-PLA) materials. It is recognizable in the subsequent sections discussed below that researchers have now expanded their employed techniques to realize inorganic nanostructures with improved placement accuracy and pattern uniformity.

3.2. Atomic layer deposition methods and block copolymer templates

ALD is a versatile technique for depositing inorganic materials for the controlled formation of uniform layers via vapor phase precursors.[91] The systematic nature of ALD cycles enables

atomic level precision through self-limiting surface reactions in the deposition of inorganic functional material. Such approaches allow tuning and interface engineering to precisely modify nanoscale BCP features on a large scale. This review focuses on techniques that modify nanolithography relevant self-assembled BCP templates (spheres, cylinders, lamella) as opposed to methods that coat or infiltrate kinetically trapped structures like micelles,[92] nanorods,[93] *etc*. It could be argued that ALD alone is not a true "infiltration" technique however it warrants highlighting due it possible impact for feature size alteration, density multiplication potential and close relationship with SIS (Section 3.3).

A variety of ALD-BCP practices have emerged that could continue the scaling of complementary metal-oxide semiconductor (CMOS) devices in the future. An interesting article in 2014 by Moon *et al.*[94] introduced a methodology combining ALD alumina coating and a porous PS template (initial periods of 46 nm and 28 nm) to reduce and define periodicities of 14 nm in line space patterns with feature sizes of ~ 5 nm whilst the approach can also lead to period and feature size shrinkage for hole patterns. **Figure 6** shows SEM images of reduced features enabled through ALD spacing layers. The methodology possesses great potential for circumventing the size limitations associated with low χ BCPs like PS-*b*-PMMA. The enhancement strategy avoids costly lithographic tools and complex processes (such as litho-etch-litho-etch) for pattern multiplication. A uniform 5 nm thick alumina layer was deposited on the PMMA removed PS-*b*-PMMA features (lamellae for line space features and perpendicular cylinders for nanohole arrays). This spacer layer was subsequently removed using controlled ICP etching. Additional PS removal and pattern transfer of the robust alumina features resulted in silicon line arrays and nanotubes as shown in Figure 6. A similar ALD-BCP approach albeit with larger periods (36 nm) in an earlier reported work in 2010 by researchers at CEA LETI (Grenoble, France) demonstrated the selective removal of PMMA

from PS-*b*-PMMA BCP combined with an ALD deposited alumina material to act as a hardmask.[95],[96] Through careful tuning of PS surface chemistry, alumina deposition was predominantly formed in the porous regions between PS features. The alumina patterns were then pattern transferred to the underlying substrate producing high-fidelity silicon nanostructures (Figure 6g and h). In the above works, the benefits offered by inorganic inclusion via ALD are clear for density multiplication [94][94][94][94][94]and enhanced pattern transfer, and it is worthy to note the importance and understanding of dry plasma etching processes tailored for transferring the ALD generated features.

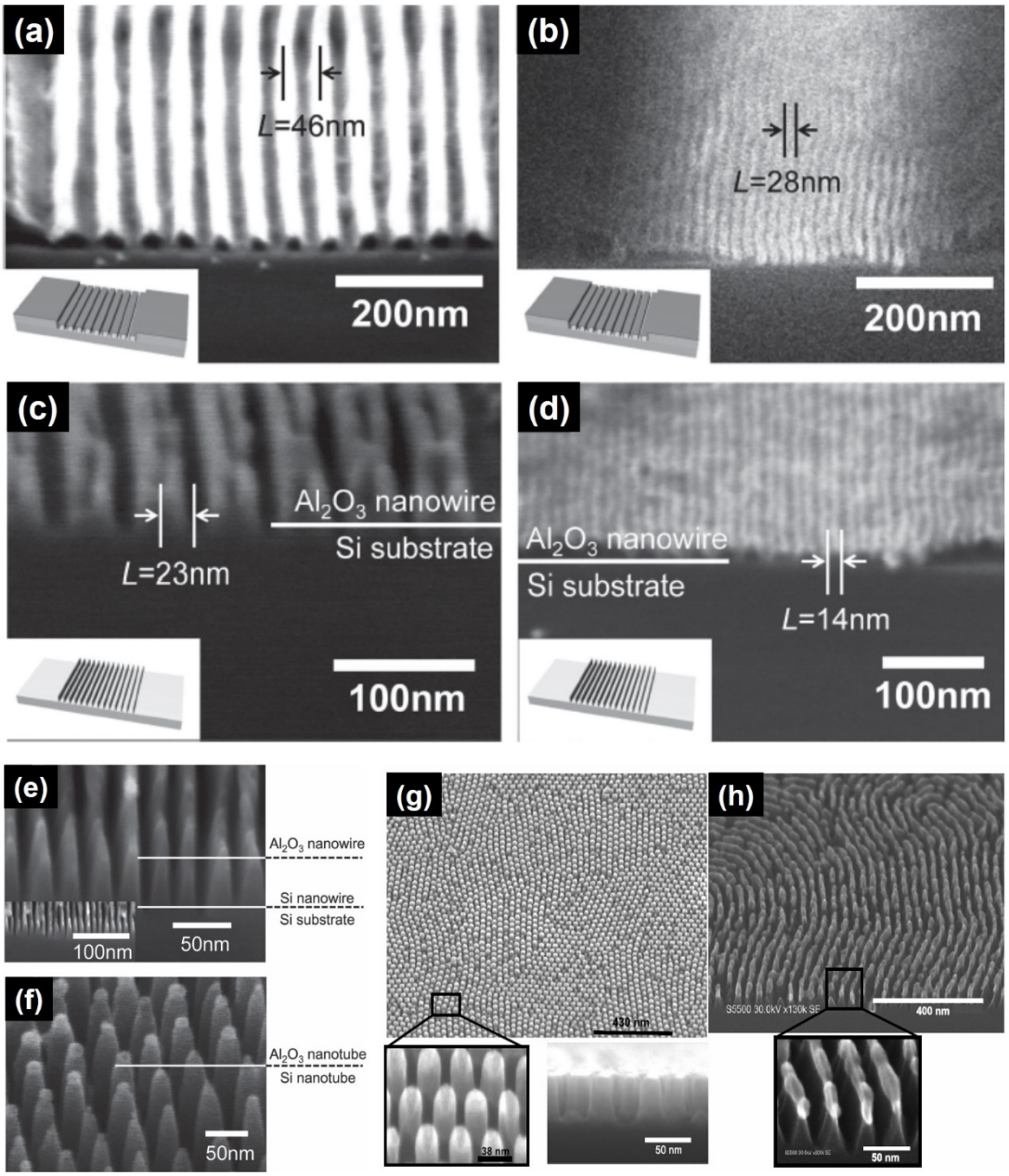


Figure 6. Side-view SEM images of PS line space templates from PS-*b*-PMMA BCPs with periods of a) 46 nm and b) 28 nm respectively. Corresponding alumina nanowire features following ALD spacer deposition, ICP spacer etching and BCP etching producing reduced features at c) 23 nm and d) 14 nm periods. e,f) Si nanostructure and nanotubes after Si etching. Side view and high resolution SEM images of g) nanopillars and h) nanofin features using robust ALD Al_2O_3 mask patterns for enhanced pattern transfer.

In 2013, a work by Hagglund *et al.*[97] utilized a BCP lift-off approach similar to studies reported in section 3.1 to pattern high density arrays of Au nanodots and SnS_x or ZnO ALD films were subsequently deposited on the arrays. The ALD deposition was carried out to enhance and analyze the optical effects of the plasmonic arrays. The authors reported a record effective absorption coefficient per volume equivalent thickness which surpassed any previously detailed materials. The work displayed the importance of complementary methods and interdisciplinary study to achieve new fundamental insights at sub-10 nm feature sizes accessible with BCP patterns.

ALD can also been used impressively for inorganic replication of highly oriented thicker BCP templates with great precision. For example, using 500 nm porous PS-*b*-P2VP films Yin *et al.*[98] created titania nanotubes as shown in **Figure 7**d and e. An important process step for this accomplishment is related to the "reactivity" of the PS-*b*-poly-x-vinylpyridine (x = 2 or 4) containing BCPs. As mentioned in section 3.1, when exposed to selective solvent PVPs swell and form pores. Depending on conditions, *viz.* time and temperature, the pore size can be tuned and therefore one can alter the diameter of included precursor via pore size tuning as well as precursor loading. Such deep micron thick, well-ordered inorganic features from BCP templates with high porosity may have potential in a number of catalytic, sensor and separation

science areas. The approach has been used to deposit metal oxides within membrane features for antireflective application[99] and nanorods for enhanced humidity-sensing[100] designed from PS-*b*-P2VP BCPs. Synthetic methods have advanced endlessly to add functionality to BCPs[16] and BCPs containing an easily removable block to form nanoporous templates for deposition are advantageous. A recent study published illustrates this synergy of BCP functionality and ALD patterning. Initially, a Si containing BCP, PS-*b*-(4-(tert-butyldimethylsilyl)oxystyrene) (PS-*b*-PSSi)[101] was synthesized and solvent vapor annealing produced PS nanodot arrays surrounded by a majority PSSi matrix (see Figure 7f-j). The natural etch contrast of the PSSi allowed selective PS etching to create a nanoporous PSSi template with ~ 200 nm thickness on an organic resist material (SU-8).[102]

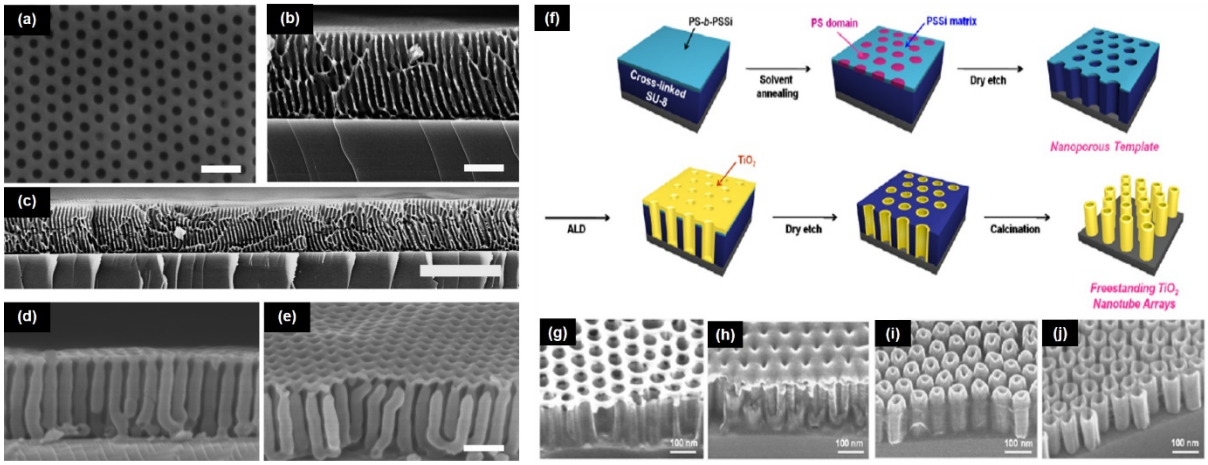


Figure 7. a-c) 500 nm porous PS-*b*-P2VP nanodot features used as host template for ALD TiO_2 nanotube fabrication (d, e). f) Scheme for TiO_2 nanotube arrays using PS-b-PSSi BCP template. g) Nanoporous PSSi template, h) after ALD of 20 nm TiO_2, i) after dry etch step, and j) freestandingTiO_2 nanotube array following calcination to remove organic matrix material.

Following pattern transfer of the nanopore arrays to the thick underlying cross-linked SU-8 layer, sequential ALD processing and calcination led to highly ordered crystalline anatase titania. Nanolaminate ($TiO_2/Al_2O_3/TiO_2$) and mixed phase (Ti-O-Ti) nanotube arrays were

also fabricated. The work demonstrated a robust manner for creating hybrid materials circumventing the problematic nature of commonly employed AAO templates that can suffer pattern collapse.

Recently, a functional route combining directed block copolymer self-assembly and ALD was employed to create reduced features of a PS-*b*-PDMS.[103] Tolbert and co-workers described how through using repeated ALD cycles of alumina they reduced spacing of PDMS cylinders from 20 nm to less than 10 nm. The modification allowed the spin coating and alignment within ALD coated PDMS cylinders of 1-D FePt nanocrystals, a useful magnetic material (**Figure 8**). As highlighted in the work, the ALD coated layer behaves as a protective layer to the underlying polymer pattern since the organic solvents used to spin coat FePt nanoparticles would generally destroy the polymer. Additionally, the alumina layer provides thermal stability (up to 250°C) that allowed FePt particles to exhibit both ferromagnetic and superparamagnetic behavior. The work illustrated the flexibility that DSA of BCPs provides to address not only nanolithographic issues but to enable high density alignment of magnetic material.

As mentioned above, another factor to consider for achieving high control, uniformity and precision of inorganic incorporation is the use of easily etchable blocks in a BCP to create a porous host material. In this regard, one of the best BCPs studied to date has been PS-*b*-poly(lactic acid), also referred to as PS-*b*-polylactide (PS-*b*-PLA).[104] Owing to the degradable PLA component, porous templates can be formed through simple wet etching. Ming-Ho and co-workers have produced excellent 3-D inorganic replicas (*e.g.* silica,[105],[106],[107] titania[108]) with PS-*b*-PLA gyroid templating structures via sol-gel reactions for environmental use, drug delivery application and anti-reflection purposes. The work has been reviewed extensively.[104],[109] Recently, Gladfeltera and co-workers have published work[110] employing

ALD ZnO to achieve smaller feature dimensions using PS-*b*-PLA in a similar fashion to work described above.[103] However, this work involved using a porous majority PS matrix template (Figure 8a) generated from a hexagonal forming PS-*b*-PLA BCP to reduce the pore size of perpendicular cylinders. After successfully reducing pore diameter from 30 nm to 14 nm (Figure 8b and c), permalloy ($Ni_{80}Fe_{20}$) was evaporated on the ZnO "nanocrucibles" followed by a "Damascene-type" process reported earlier[90] to leave well-ordered ZnO nanocrucibles surrounding the permalloy dots. The material showed ferromagnetic multidomain/vortex state at larger diameters but at reduced diameters (14 nm) exhibited superparamagnetism.

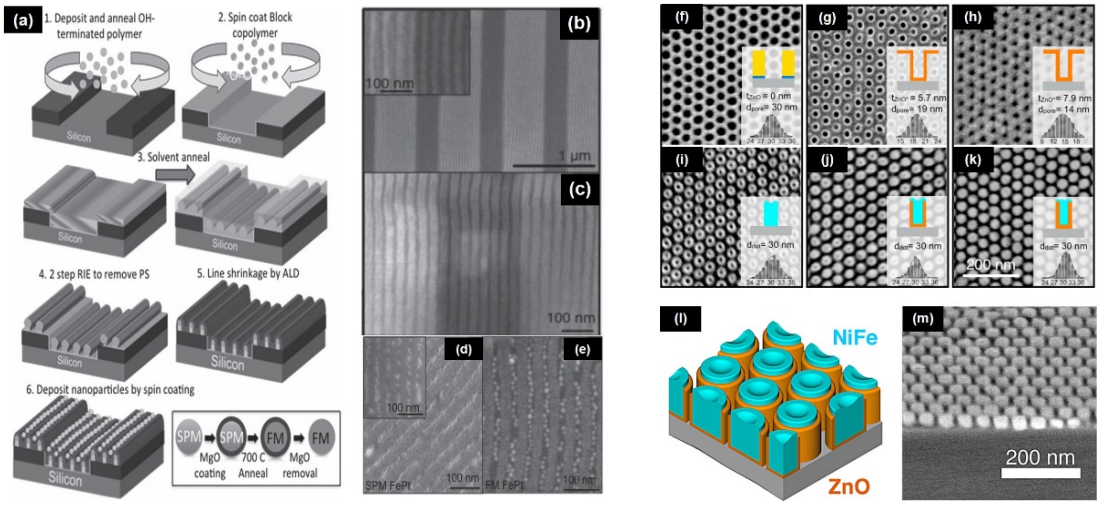


Figure 8. a) Process flow for line shrinkage of PS-*b*-PDMS BCP by ALD methodology. b) DSA of line features. c) Reduced line features following 40 cycles of alumina ALD. d) Aligned superparamagnetic FePt nanocrystals. e) Aligned ferromagnetic FePt nanocrystals. f-m) Top-down SEM images of reduced nanodot tuning through repeated ALD ZnO cycles. f) Nanoporous PS template after PLA removal, g) 5.7 nm ZnO coated with a pore size of 19 nm and h) 7.9 nm ZnO coated with a pore size of 14 nm. i-k) Corresponding permalloy filling of ZnO nanocrucibles. l) Graphical representation of ZnO nanocrucibles filled with permalloy material. m) Side-view SEM of k).

The combination of BCP nanolithography and conformal coating through ALD enabled high temperature processing to be carried out that might have use for bit patterned media application. As stated earlier, most reports using ALD on copolymer structures have focused on non-linear architectures. This section illustrates the significance of emerging work on the utilization of ordered DSA related BCP patterns coupled with ALD patterning to achieve not only nanolithographic triumphs but also the optimization of the two processes to access alignment of relevant magnetic material and highly porous inorganic designs with potential ultrahigh density bit media, solar cell, environmental and photochemical applications.

3.3. Sequential infiltration synthesis of block copolymers

Peng *et al.*[111] were the first to employ an ALD derived process (in later publications coined sequential infiltration synthesis or SIS) with an asymmetric forming PS-*b*-PMMA BCP system consisting of either nanoposts or cylinders to fabricate metal oxide arrays. As depicted in **Figure 9** and **Figure 10**, the process involves initial exposure of the PS-*b*-PMMA films to precursor molecules (trimethyl aluminum or titanium tetrachloride/water) possessing an affinity to the reactive PMMA domain. These domains behave as growth sites for subsequent ALD cycles that can be infiltrated with an array of semiconductor and light active materials. It can be noted that the alternative strategy used here avoids using UV exposure/acetic acid washing process described earlier for PMMA elimination although the PMMA microdomains are still of infiltration interest. In this first publication in 2010, Al_2O_3 and TiO_2 arrays were generated using ALD cycles and feature sizes beyond the original polymer template were enabled through repeated ALD cycles as well as longer precursor exposure times. There are two key achievements through this synergistic ALD-BCP approach. Firstly, the methodology is based on forming inorganic structures within BCP domains rather than at interface boundaries. This is in contrast to other work that coats the outside of polymer materials with

ALD. Furthermore, block removal is not necessary and thus an often problematic process step such as wet etching that can induce defects is avoided. In this respect, it may be possible to apply the methodology to reactive sites in BCPs which do not contain an easily removable block. Secondly, the methodology allows a facile way to mimic the original BCP nanopattern without disturbing morphology. Peng's work employed already assembled BCP domains and chemically enhanced the domains via "molecular recognition". The ability to tune and alter the resulting feature sizes without having to adjust the BCP molecular weight is advantageous. However, although SIS provides scope to alter feature sizes one would assume there are upper and lower thresholds for feature size tuning. We state this as presumably at later stages after repeated cycles or higher precursor loads, infiltrated domains may agglomerate during feature formation.

In a follow-up work, Darling, Elam and co-workers demonstrated the fabrication of continuous ZnO, SiO_2 and W line structures with SIS and PS-*b*-PMMA BCP.[112] The application of the SIS practice to such a well-studied BCP system like PS-*b*-PMMA further enhances its possible integration for etch-mask applications, as the metal oxide can be employed as a hardmask to pattern the underlying device material. It is accepted that the etch contrast between PS and PMMA is relatively low and thus this chemical infiltration is an advancement with regard to device processing. Figure 9b-d shows high-fidelity silicon nanostructures perpendicular and parallel to the substrate plane following pattern transfer using an Al_2O_3 hardmask via SIS.[113]

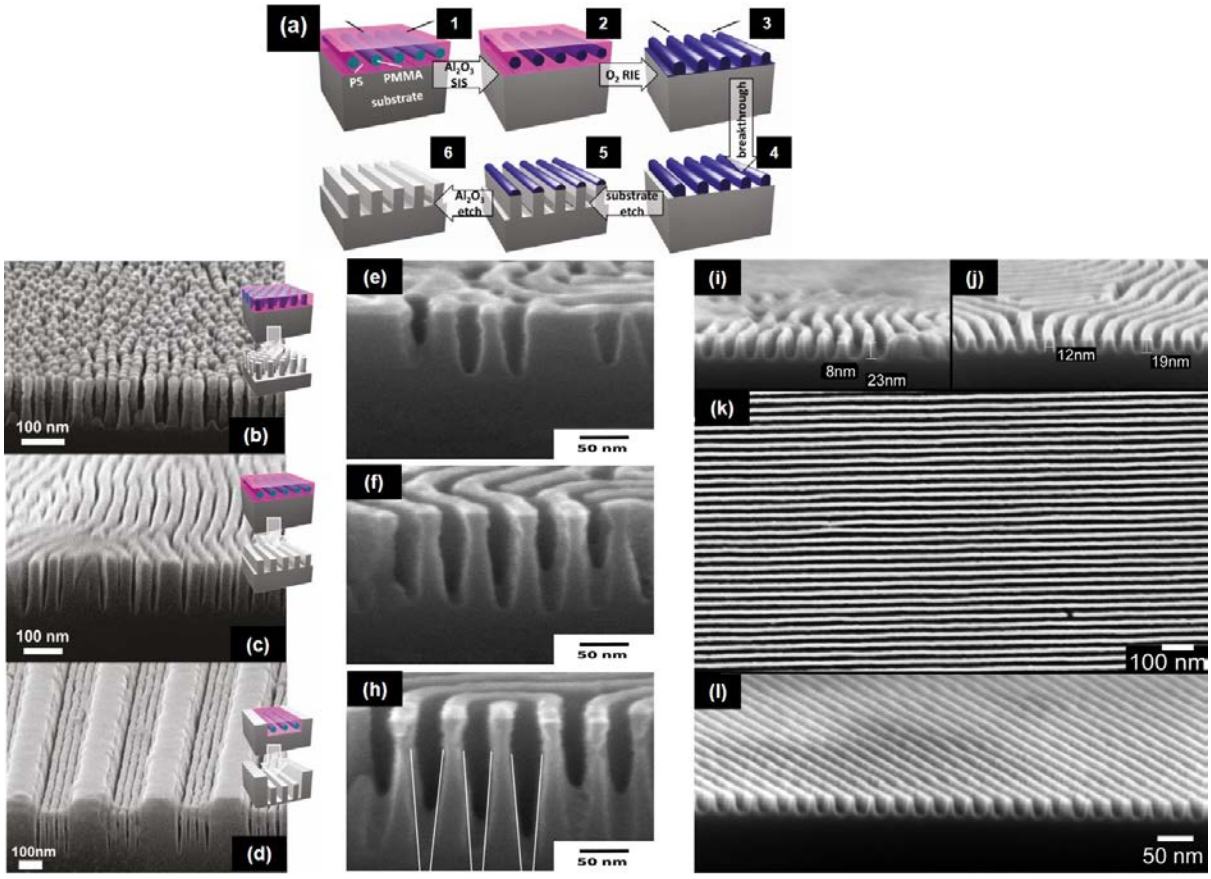


Figure 9. a) Process flow for SIS of PS-*b*-PMMA BCPs to enhance etch contrast. b-d) Cross-section SEM images of silicon nanoposts and nanofins (graphoepitaxy approach) from SIS Al_2O_3 mask for enhanced etch contrast. e-h) Patterned silicon from SIS Al_2O_3 mask using lamellar forming PS-*b*-PMMA (period ~ 38 nm) BCP system. i-l) High quality pattern transfer using SIS Al_2O_3 masks coupled with chemoepitaxy schemes for alignment.

Subsequently, Black and co-workers illustrated high-aspect ratio pattern transfer using the same SIS approach for PS-*b*-PMMA (see Figure 9e-l).[114] Systematic studies were carried out analysing the Al_2O_3 infiltration effect on domains which showed that image quality suffered with higher ALD cycles.[115] They also found that extensive trimethyl aluminium/water exposure cycles or ALD cycles alone damaged the pattern quality. Another report provided a further advance and twist on the SIS technique by simply exposing PS-*b*-PMMA BCPs (cylindrical and lamellar morphologies) to UV light for a short period thus creating activation

of reactive sites for precursors.[116] However, the reactive sites in this case were in the PS component of the BCP in comparison to the PMMA block as described earlier. This simple modification allowed selective infiltration to an alternative block other than PMMA. The ability to switch from PMMA domain infiltration to PS domain infiltration creates further opportunities for the SIS methodology to be adopted. The most prominently studied BCPs other than the "first-generation" PS-*b*-PMMA BCP contain a PS block in most cases *e.g.* PS-*b*-PEO, PS-*b*-PDMS, PS-*b*-P2VP, PS-*b*-P4VP and PS-*b*-PLA. The fabrication of different metal and inorganic nanopatterns by SIS using different BCPs and their applications are listed in Table 1. For this reason, alternative block selectivity could be used to achieve inverse nanopatterns.

Impressive reports by Checco *et al.* [117],[118] and Rahman *et al.*[119, 120] has already shown the near future commercial potential of infiltrated BCP technology for everyday use. In one report, Al_2O_3 features produced via SIS coupled with evaporation and vapor synthesis have been utilized to produce Fe, Si and Ge nanowires for anti-reflection and hydrophobic application.[120] In another work, following the fabrication of cone tipped nanopillars (Figure 10c) superhydrophobicity was observed over large areas.[117] Superhydrophobicity describes the ability of a rough hydrophobic surface to repel water, with criteria including a contact angle greater than 150° and low roll-off angle/contact angle hysteresis. Superhydrophobic surfaces designed in this manner hold potential for commercialization however further research in their design to improve overall stability could have serious outcomes for self-cleaning surfaces and energy/heat conservation.[121] The researchers initially formed hexagonally packed PS-*b*-PMMA BCP patterns over large areas. The patterns were then infiltrated with Al_2O_3 and subsequently pattern transferred to the underlying substrate. Using a highly selective etch that created a tapered sidewall due to lateral silicon etching, water droplet behavior was investigated. Prior to the water droplet testing, octadecyltrichlorosilane was coated on the

different topographies created (spacing varied from 30 – 52 nm for both nanopillars and nanocones). The tapered cone nanopillars proved to be the optimal geometry for superhydrophobicity.

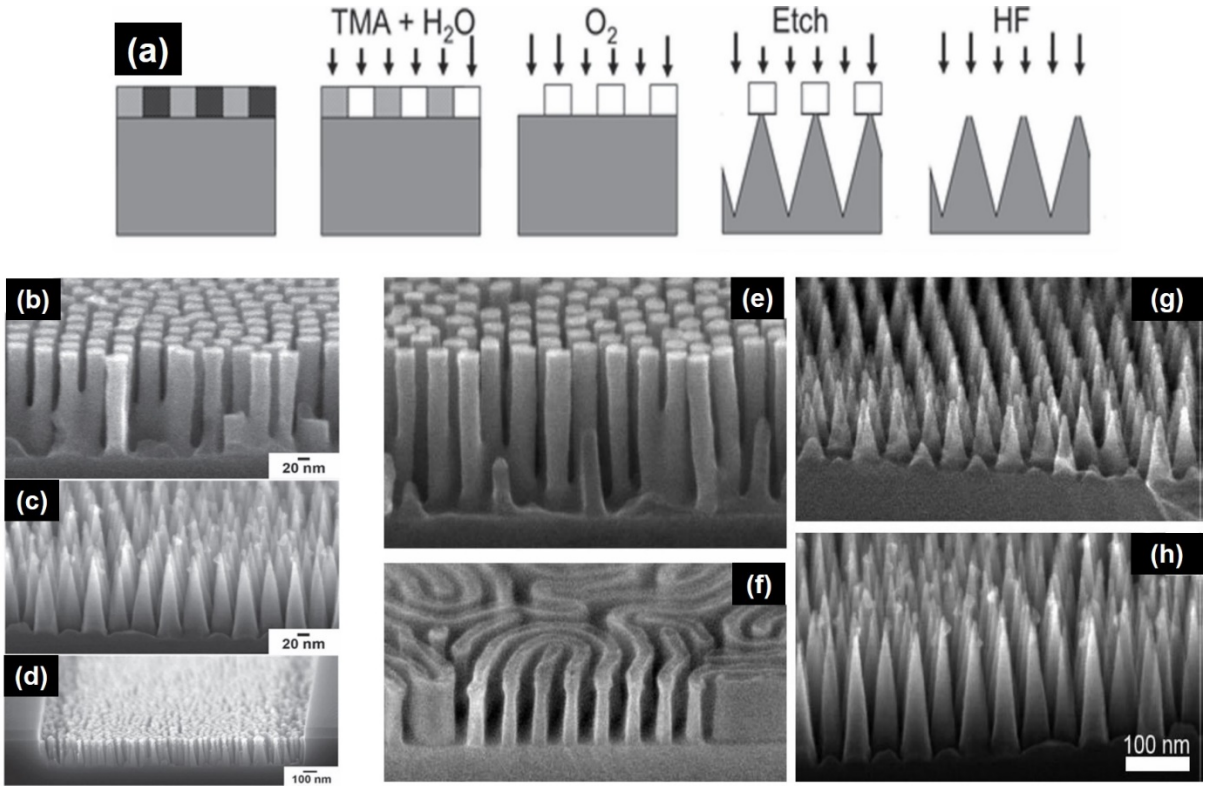
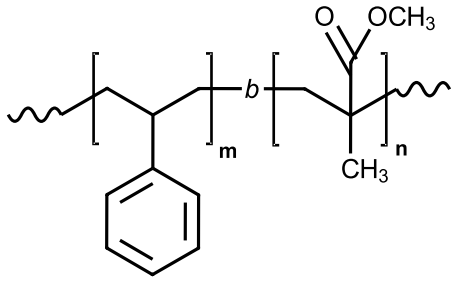
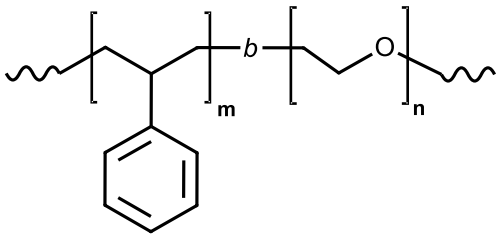
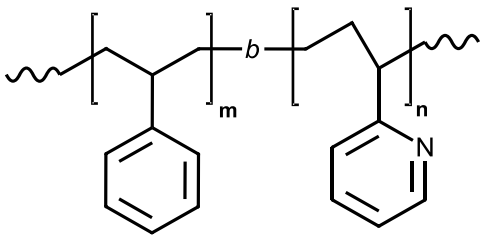
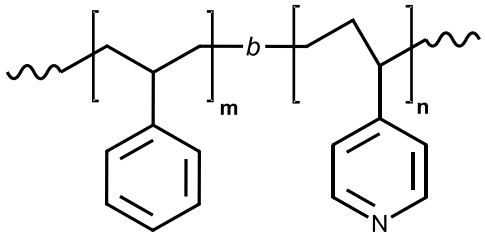
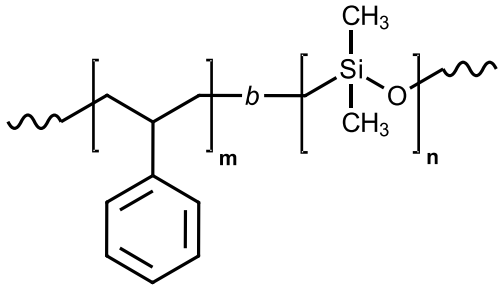
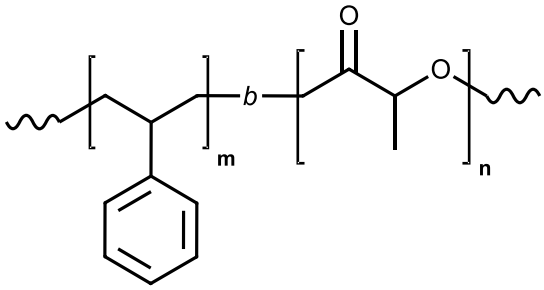


Figure 10. a) SIS process flow of PS-*b*-PMMA BCP, followed by plasma and wet etching for nanocone fabrication. b-h) Cross-section SEM images of silicon nanofeatures patterned using SIS Al_2O_3 of PS-*b*-PMMA BCPs (cylinder and lamella) for superhydrophobic application. e-g) Scale bars = 100 nm.

Table 2. Block copolymers, infiltration techniques and reported functions

Block Copolymer	Infiltration Technique	Resulting Nanostructure	Function/Application
PS-*b*-PMMA 	Evaporation/E-beam or Ion beam deposition	Au dots/posts,[53, 55, 60, 80, 97] Co posts,[58] Co nanorings,[61] Fe posts,[63] Cr posts[59, 73] aligned Al and Au nanowires,[64] Ge nanowires,[68] Al_2O_3 dots,[66] Ti/Pt dots[85]	On-chip etch mask,[44] ferromagnetic nanorings,[61] carbon nanotube growth,[63] metal nanodot memory device,[73] triboelectric generator,[62] resistive switching nanodevice,[85] plasmonic,[97]
	Atomic layer deposition	Al_2O_3 line and hole spacer,[94] Al_2O_3 wires and posts [95, 96]	On-chip etch mask[96]
	Sequential Infiltration Synthesis	Al_2O_3 posts,[111],[116],[117],[118],[119],[120],[122] Al_2O_3 wires, [111],[112],[113, 114],[115],[116] TiO_2 wires,[111] SiO_2 posts,[112] SiO_2 wires,[112] W wires,[112] ZnO posts,[116] ZnO wires[112, 116]	On-chip etch mask,[113],[114],[115],[117],[118] SIS procedure for PS block selectivity,[116] superhydrophobicity,[117, 118] anti-reflection,[119] nanowire growth,[120] broadband antireflection for Si solar cell[122]
	Spin coating	FePt nanoparticles,[123, 124] CdSe nanoparticles,[124] CdSe@ZnS quantum dots,[125] Fe_2O_3 nanoparticles,[125] 1D ZnO nanorods[125]	Alignment of nanoparticles within BCP grooves, [100,101,114] dual nanopatterning[125]
PS-*b*-PEO 	Metal Salt Inclusion	Fe_2O_3 dots, [126],[127],[128],[129] Fe_3O_4 dots, [126],[127],[128],[129],[130] CeO_2 dots, [128, 131] CuO dots,[128] lead zirconate titanate dots,[132] Ag dots[133] Fe_2O_3, Fe_3O_4 wires[134]	On-chip etch mask,[127],[128],[130] superparamagnetism,[126, 129] vertical Si nanowires for neuroelectrode modification,[130] ferroelectric,[132] antimicrobial function[133] On-chip etch mask[134]
PS-*b*-P2VP 	Atomic layer deposition Precursor spin coating	TiO_2 nanotubes[98] SiO_2 posts[75]	500 nm thick porous TiO_2 nanotubes[98] On-chip etch mask, SiO_2 pillars[75]
	Aqueous metal reduction	Au, Pd, Pt, Fe, Co, Cu, Ni wires[135],[136],[137]	Aligned metallic lines and density doubling using graphoepitaxy,[135], [136],[137]electrical resistivity of Pt wires[135]

PS-*b*-P4VP 	Sputtering	Au decoration[72]	On-chip etch mask, Patterned SiO_2 posts, pillars and rings[72]
	Metal salt inclusion/precursor spin coating	Fe_2O_3 dots,[138] Fe_3O_4 dots,[138] Fe_3O_4 and Al_2O_3 wires,[139],[140] HfO2 wires,[141] SiO_2 posts,[75, 142] SiO_2 wires[142]	On-chip etch mask - Si nanopillars,[138] Si and Ge nanofins,[139],[140],[141] SiO_2 pillars[75]
	Aqueous metal reduction	Fe_2O_3 nanoparticles,[143] Au dots, Pt dots, Pt/Au dots, Au wires/Au dots, Au wires/Pt dots, Pt wires/Pt dots,[144] Fe-Pt, Co-Pt, Pd-Au, Co-Pd-Pt alloys,[145] Au rings, dots, meshes, double wires,[146] Au wires and meshes[147]	Carbon nanotube growth,[145] charge trap memory device,[144] plasmonic[144, 146]
PS-*b*-PDMS 	Sputtering	Ti,[86] W,[86, 87] Pt,[86] Co,[86], Ni, [86] Ta,[86] Au,[86] Al,[86] Ti wires[89] Co double rings[88] Pt, W, Ti, Ta, Ni dots [89]	Graphoepitaxially aligned inorganic wires[86, 87] Electrical and magnetic Ni nanowire properties[86] Nanopore on-chip etch mask[89]
	Atomic layer deposition	Al_2O_3 feature reducer[103]	Alignment of FePt nanoparticles[103]
PS-*b*-PLA 	Molecular beam deposition/evaporation	$Ni_{80}Fe_{20}$,[90],[110] Ni[74]	Ferromagnetism[90],[99]

A notable report in 2015 showed that the silicon nanotextures could be utilized for solar cell application. Specifically, Rahman *et al.*[122] described that enhanced broadband antireflection in silicon solar cells could be achieved using silicon features with sub-50 nm fabricated via SIS alumina infused PMMA domains of a PS-*b*-PMMA BCP. The practice involved is a facile and low-cost device route to surpass common bulk materials with antireflective silicon nitride coating layers.

Despite the experimental evidence demonstrated thus far for the efficacy of SIS treated materials, little clear understanding of the mechanism(s) has been put forward until now. Using *in-situ* Fourier transform infrared analysis, Biswas *et al.*[148] ascertained that a two-step mechanism is involved leading to the formation of covalent bonding between carbonyl group of PMMA and aluminium precursor. In general, the first step of SIS involves the exposure of polymer material to TMA. This was found to an extremely quick interaction (180 seconds) but is quite unstable. The formation of stable Al-O linkages will subsequently occur in a slow manner (close to ~ 60 minutes) but is dependent on TMA desorption. Once a high concentration level of the initial physisorbed complex (TMA-C=O) exists, stable covalent Al-O bonds will form. The author's hypothesis on intermediate complex formation was also confirmed by density functional theory calculations. The most significant comment in their study is "*that the TMA purge time is crucial for Al_2O_3 formation within PMMA*". This is related to the unstable nature of the TMA-PMMA interaction and that short purge times are required in order to augment the formation of Al_2O_3 in PMMA growth sites. A comprehensive insight of the SIS process in relation to PMMA film thickness and temperature effect was also reported.[149] Such studies to define and understand the complex molecular level interactions are extremely useful if SIS BCP nanolithography methods (and SIS e-beam, optical resists[150],[151],[152]) are to be commercially viable for HVM and VLSI where stringent defect tolerance levels must be satisfied.

3.4. Spin coating methodologies for metal nanoparticle alignment and metal oxide inclusion with "activated" block copolymer templates

Spin coating inorganic nanoparticles is an attractive approach for generating functional features as many routes possess the potential for industrial scale processing. Spin coating on modified

(*e.g.* photochemically altered, selective solvent swelling) BCP thin films combined with further treatment (*e.g.* thermal annealing, calcination, UV/ozonation) can lead to semiconductor, ferroelectric or magnetic materials in a highly straight-forward process. In 2005, Darling *et al*.[123] demonstrated a novel route for the placement of magnetic FePt nanoparticles on vacuum ultraviolet etched PMMA half-cylinder domains in PS-*b*-PMMA system as shown in **Figure 11**. The etched PMMA domains provided a selective channel for oleic-acid capped FePt nanoparticles. Importantly, the resulting functional material length scale was an order of magnitude smaller the initial PS-*b*-PMMA template. Darling's work showed the simplicity of spin coating functional material on modified BCP templates.

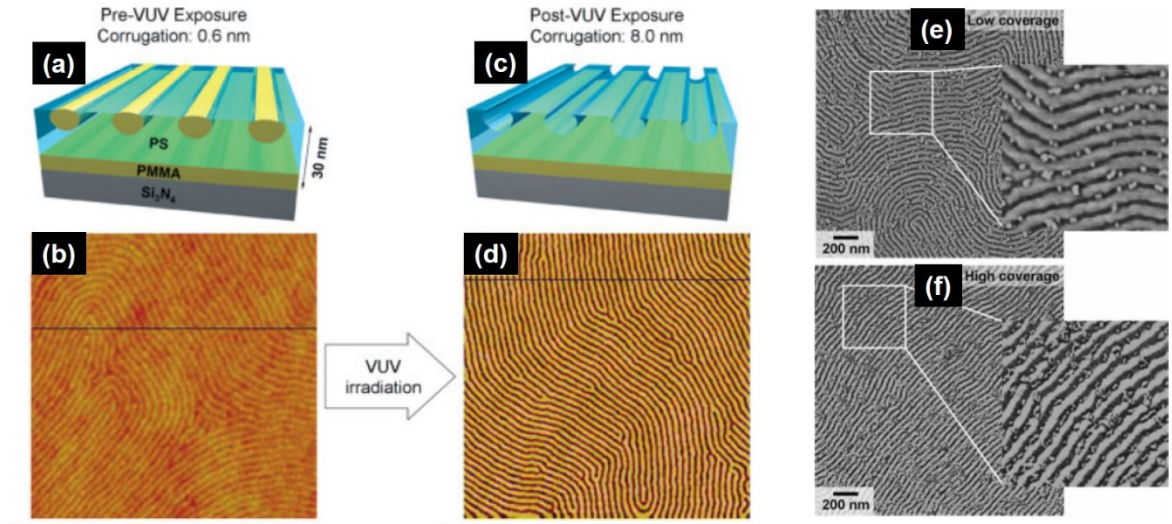


Figure 11. a-c) show schematic representation of cylinder forming PS-*b*-PMMA films before and after VUV irradiation used to etch PMMA half-cylinders. (b) and (d) are corresponding AFM images (both 2 x 2 µm). Following spin-coating of FePt nanoparticles low coverage (e) and high coverage (f) areas of nanoparticle clusters were identified showing high adsorption to the photochemically altered PMMA domains.

Moreover, the work highlighted the potential and significance of altering chemistry of self-assembled BCP templates for creating "nanotroughs" and domains for the positioning of

nanomaterials. Additional work[124] suggested that the process was physical rather than chemical which expanded the range of nanoparticles that could be aligned in etched microdomain channels.

In 2009, Son *et al.*[125] demonstrated a facile spin-coating process for the placement of nanomaterial including CdSe@ZnS quantum dots, Fe_2O_3 nanoparticles, and 1-D ZnO nanorods after exposing PS-*b*-PMMA patterns to selective solvents creating surface reconstructed grooves. The authors also managed to create dual patterned films (consisting of CdSe@ZnS quantum dots and Fe_2O_3 nanoparticles) through electron beam exposure following the first nanoparticle deposition step. One should note the progress of placement and alignment in the recent synergistic approach[103] detailed in section 3.2. for FePt nanoparticles utilizing ALD modified DSA BCP patterns.

More recently, we have demonstrated a rich variety of metal oxide nanostructures with as-formed self-assembled cylinder forming PS-*b*-PEO and PS-*b*-P4VP BCPs through an "*in-situ*" metal-salt inclusion spin coating methodology. Since cylinder systems can be tailored to enable perpendicular or parallel cylinder orientation through solvent vapor annealing treatment, both metal oxide nanodots and nanowires can be accessed. Initially, neat PS-*b*-PEO or PS-*b*-P4VP templates with enhanced ordering are modified and "activated" through ethanol treatment. The PEO and P4VP block selectivity's to ethanol render nanoporous templates for successful metal ion inclusion. Whilst the exact mechanism of pore forming is under debate for these systems, evidence suggests that PEO domains are partially etched or modified.[134] In contrast, P4VP domains are swollen and collapse within the pores as others have noted.[98] The treatment is proven to be reversible through appropriate treatment for PS-*b*-P4VP BCPs.[72] The "activation" step is crucial for allowing the inorganic salt to be included in the desired location.

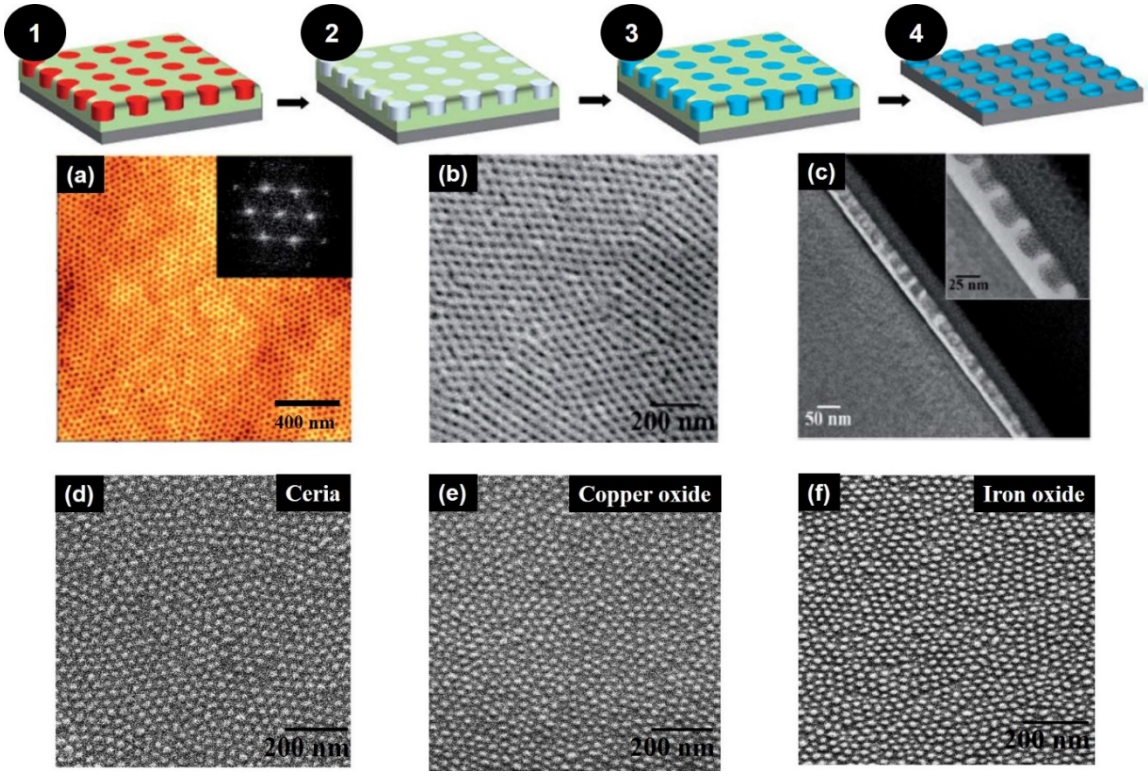


Figure 12. Process involving "activated" BCP nanodot features and metal salt inclusion to form metal oxide nanodot arrays. (1) Self-assembled PS-*b*-PEO BCP nanodot pattern following solvent vapor annealing. (2) "Activated" film formation after immersing in ethanol. (3) Metal ion inclusion via spin coating on "activated" PS-*b*-PEO nanodot template. (4) Metal oxide nanodots after inclusion and UV/O_3 to oxidize metal ion and remove polymer matrix. (a) AFM image of microphase separated PS-*b*-PEO film. b,c) SEM image and TEM cross-section image of nanoporous PS matrix following "activation" using ethanol. SEM images of a) ceria, b) copper oxide and f) iron oxide nanodot arrays following metal salt inclusion process.

Micelle formation can be used to form metal nanoarrays;[153],[154],[155] however the associated co-ordination chemistry can be complex, particularly for BCPs not possessing a direct bonding site. Moreover, in technologies such as lithography and fluidics, pattern placement is paramount and therefore micelle formation restricts line space feature formation and high registration being achieved. The spin coating methodology we have employed translates to

both perpendicular and parallel cylinder orientations with large scale inclusion and uniformity evident. In initial works, iron oxide(s) (Fe_3O_4 and Fe_2O_3) nanodot arrays were created over large areas following spin coating of a metal nitrate ethanolic solution.[126],[138] Following deposition of the metal salt precursors by spin coating, ultraviolet/ozone treatment is carried out to remove the remaining polymer matrix material and oxidize the nitrate precursors to form metal oxide features as shown in **Figure 12**d-f. Others have recently adopted a similar approach to form oxides and then thermally annealed films post metal precursor deposition to remove the polymer template.[156] In 2008, Park *et al.*[142] demonstrated silica nanodots and nanowires following spin-coating of a PDMS precursor in selective solvents on surface reconstructed PS-*b*-P4VP films. In our work, the iron oxide nanodots produced from perpendicularly oriented PEO cylinders were shown to possess superparamagnetism as the features are less than the single domain size of iron oxide (< 20 nm).[126] The methodology has shown the ability to easily change a nanodots size through simply increasing metal ion concentration without having to change the BCP molecular weight.[128] Additionally, the practice and corresponding superparamagnetism was demonstrated for a series of high and low molecular weight PS-*b*-PEO systems.[129] Of late, hemispherical Fe_3O_4 nanodots were utilized as catalysts for germanium nanowire growth that possessed coherent twin boundaries perpendicular to the nanowire growth direction.[157] Thus far, Fe_3O_4,[129],[138],[139] CeO_2,[128, 131] CuO,[128] and Al_2O_3[139] patterning of nanodot and nanowire features have been developed using the metal salt inclusion methodology and have been shown to be effective on-chip etch masks on silicon (see examples in **Figure 13** and Table 2). Fe_3O_4 inclusion has been shown to be effective in a low molecular weight lamellar PS-*b*-P4VP system for line space features with a pitch of ~10 nm.[158]

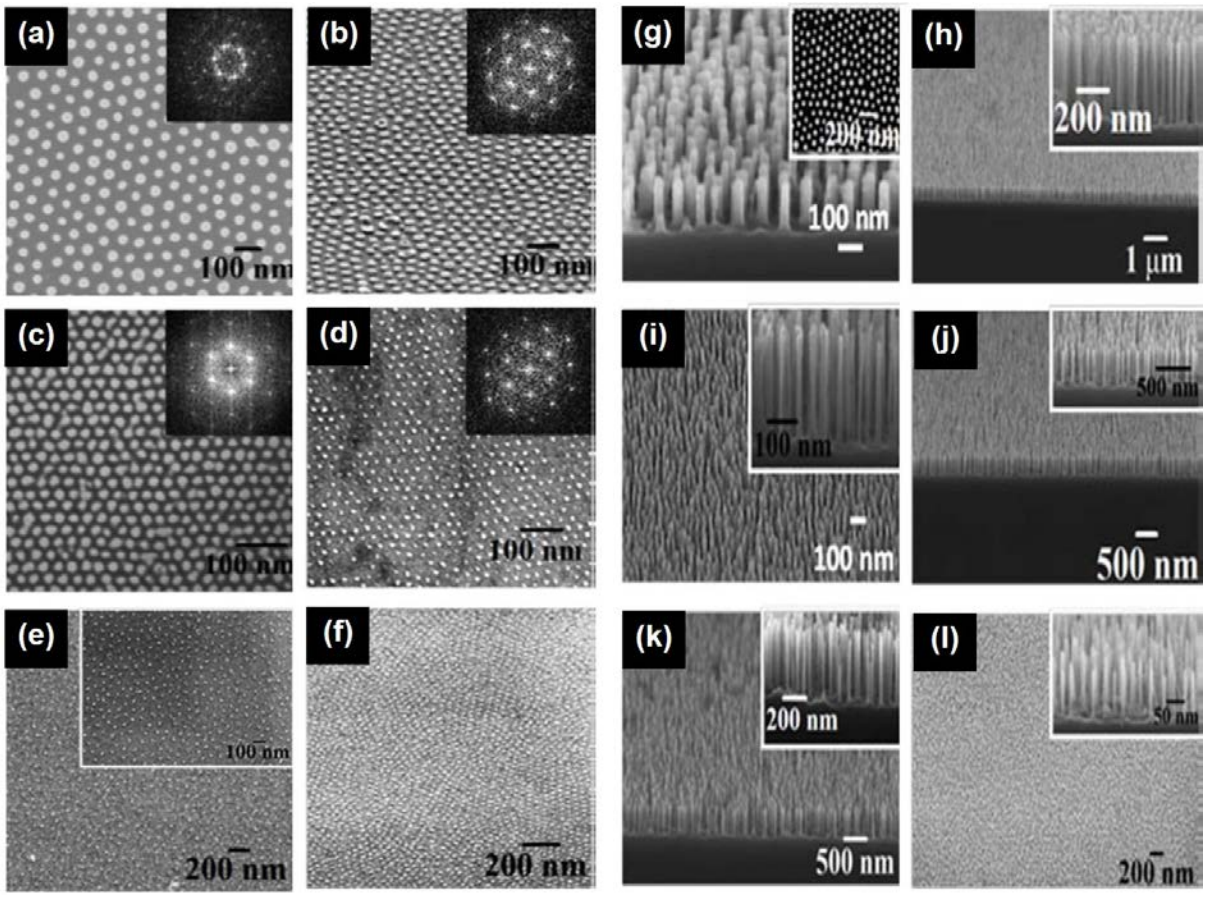


Figure 13. a-f) Series of top-down SEM images of varying Fe_3O_4 nanodots with different periods. g-l) Corresponding structures following pattern transfer of Fe_3O_4 etch masks forming high-aspect ratio silicon nanopillars. See text and table 2 for application and functions.

Silicon nanopillars of 500 nm in height can be obtained following plasma etching metal oxide nanodot patterns.[127, 129, 138] Additionally, nanowires were developed in the same way for both BCP systems, PS-*b*-PEO and PS-*b*-P4VP, resulting in highly uniform Fe_3O_4 nanowires with 42 nm (PS-*b*-PEO)[134] and 32 nm (PS-*b*-P4VP)[139] periodicity. We have also integrated the metal-salt inclusion technique in graphoepitaxy schemes with similar efficacy in PS-*b*-P4VP for patterning aligned Si and Ge nanofins as shown in **Figure 14**.[139],[140],[141] "Activated" PS-*b*-P4VP line pattern and metal salt inclusion producing Fe_3O_4, Al_2O_3 and HfO_2 nanowires have been employed as robust on-chip etch masks with similar efficacy for pattern transfer. These achievements are pertinent for DSA technology as pattern transfer fidelity is critical.

Patterning magnetic and integrated circuit features via BCP nanolithography with this process offers great potential due to the simplicity and cost-effectiveness.

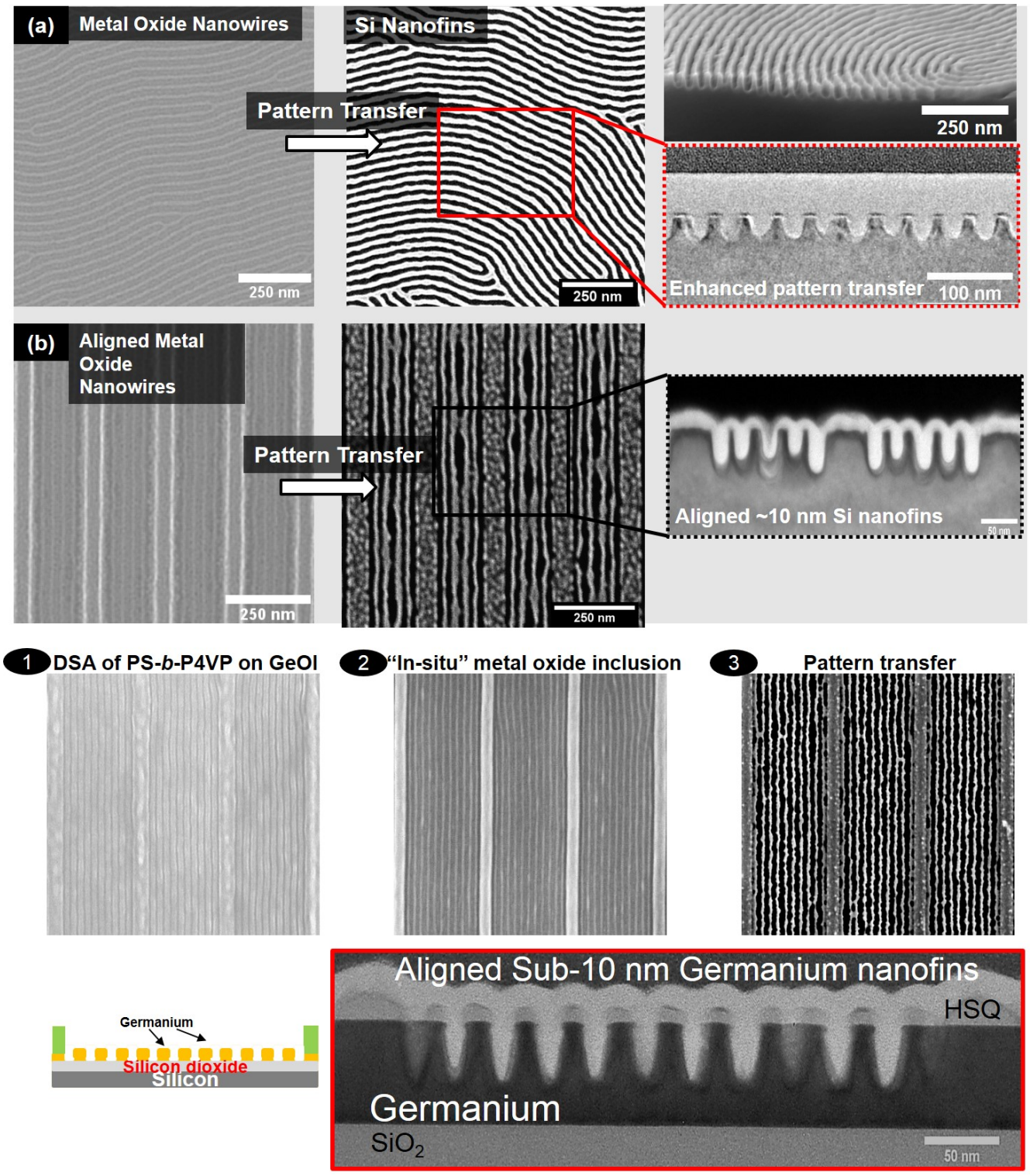


Figure 14. a) Alumina metal oxide inclusion in PS-*b*-P4VP BCP for enhanced silicon patterned transfer for line space features. b) Metal-oxide inclusion process integrated with directed self-

assembly scheme using graphoepitaxy. (1-3) Fabrication of aligned sub-10 nm germanium nanofins via metal oxide enhanced pattern transfer from PS-*b*-P4VP BCP. Note channel widths in 1-3 are 361 nm. See text for details and reference [141].

Fabrication of lead zirconate titanate (PZT) nanodots was also achieved via BCP templating that displayed piezoelectric and ferroelectric behavior.[132] The pattern density was calculated to be $\sim 68 \times 10^9$ nanodots cm^{-2}. The ability to template functional material in this fashion with ferroelectric behavior may be of use for future memory devices due to reduced power consumption and faster write speeds than flash memory.

Apart from on-chip etch mask use for achieving ultra-small feature sizes, the high-density metal and metal oxide arrays or resulting high aspect ratio pattern transferred geometries can be applied for biomedical and bioscience related applications. Recently, sub-20 nm vertical Si nanowires (generated from metal salt inclusion with PS-*b*-PEO and subsequent pattern transfer) were shown to reduce electrical impedance and increase conductivity for neuroelectrodes.[130] This is particularly useful for addressing electrode failure or deterioration as the vertical nanowires prevent tissue encapsulation of the electrode *in-situ* and, therefore, leads to longer electrode performance and sensitivity. Additionally, silver nanodots patterned on glass substrates using BCP templates have shown antimicrobial activity that may be of benefit for food packaging application.[133] Further, silver nanodots can also be used for metal assisted etching (MAE) process of Si and subsequent growth of Ge nanowires because of their thermal and chemical stability.[159] More recently, high density iron oxide nanodot arrays have been utilized for the dual electrochemical sensing of ethanol and hydrogen peroxide.[160] The above outlined inorganic nanofeature fabrication routes using “activated” BCP templates and straightforward metal-salt inclusion can access ordered arrangements of diverse inorganic

materials. The inorganic features can be pattern transferred for high-aspect ratio structures showing their etch-mask application,[127, 134] with resulting Si features also used for biomedical application[130] or inorganic features at substrate surfaces can be utilized to further efforts on magnetic,[126, 129] ferroelectric,[132]anti-microbial,[133] and electrochemical detection[160] use in an easy and low cost manner.

3.5. Aqueous metal reduction and block copolymer nanopatterns

Another route encompassing metal inclusion or more appropriately defined aqueous metal reduction (AMR) involves the immersion of BCP thin films in an acidic metal containing medium. A report in 2007 by Chai *et al.*[135],[136] using a cylindrical forming PS-*b*-P2VP BCP system and aqueous metal reduction developed highly defined Au, Pd and Pt nanowires from metal ion loading and reduction with strict alignment of the initial BCP features directed through graphoepitaxy (see **Figure 15**). Noble metal nanostructures receive much research interest as their increased scattering and absorption of light at the nanoscale can potentially be used for energy, environmental,[161] and biomedicine[162] use. The authors report that for successful metal complexation, an acidic medium is essential. Since the P2VP cylinders are buried within the hydrophobic PS matrix, access for metal ions alone is problematic. Therefore the acidic medium enabled swelling of the cationic P2VP domains which "*pierce and penetrate*" the PS overlayer. The P2VP domains eventually perforate the PS domains as shown in Figure 18 leading to mushroom caps. This perforation phenomenon can be attributed to the alteration in pH (<4.5) of the acidic medium and as noted by the authors, mushroom cap formation was more prominent with HCl (stronger acid) than HF. A follow-up work[136] reinforced the efficacy of the acidic medium for generating a morphological change in the BCP film to allow inclusion of metal ion at the protonated P2VP domains. Figure 14 shows an array of metal wires formed via immersion of PS-*b*-P2VP films in metal acidic solutions followed

by O_2 plasma treatment. Pd and other noble metal nanoparticle deposition on surface reconstructed films has been utilized by Stamm and co-workers using PS-*b*-P4VP BCP and supramolecular formed systems.[163],[164] A recent review[165] is available on the methods used which vary from deposition of pre-synthesized nanoparticles to immersion of neat films in nanoparticles.

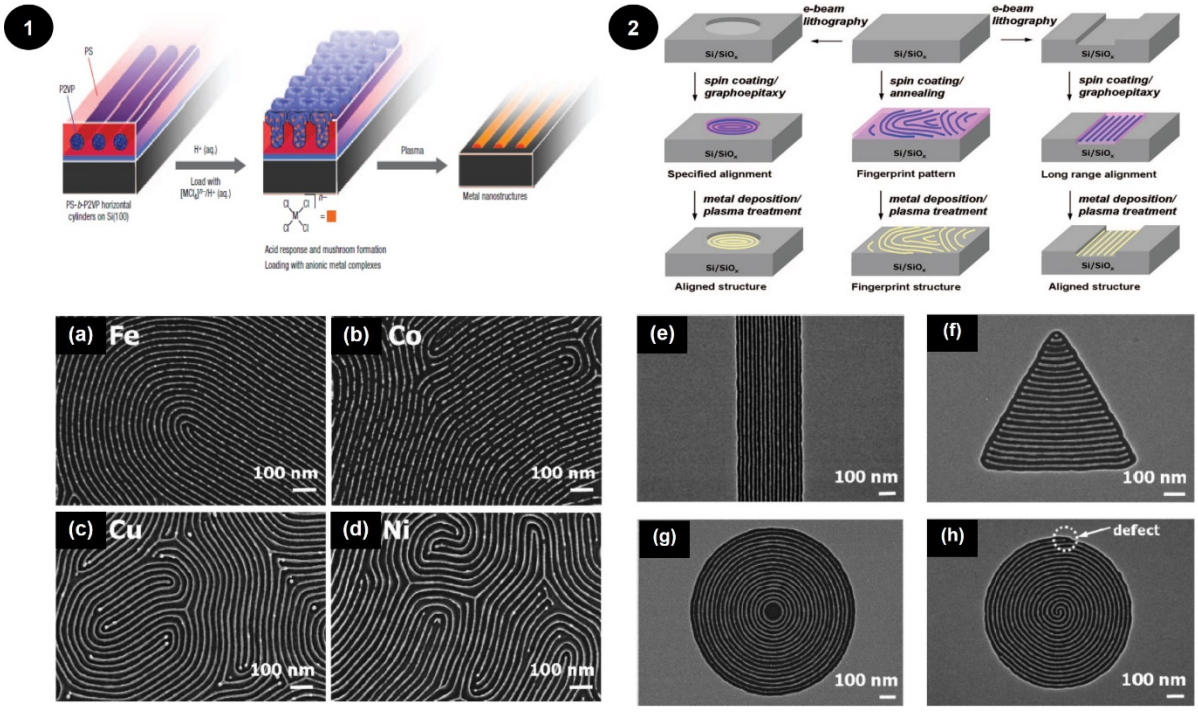


Figure 15. (1) Scheme of metal ion reduction after immersion of PS-*b*-P2VP films in acidic medium forming mushroom caps followed by O_2 plasma revealing metallic lines. (2) Process flows for graphoepitaxy approaches BCP alignment with different geometries. a-d) Top-down SEM images of Fe, Co, Cu and Ni metallic lines fabricated via aqueous metal reduction and O_2 plasma. e-h) Aligned Pt features from PS-*b*-P2VP BCP and graphoepitaxy.

Following these reports, researchers have followed a similar protocol for developing well-defined metallic features with the PS-*b*-PVP family of BCPs. One interesting publication developed monodisperse Fe_2O_3 nanoparticles via ordered PS-*b*-P4VP microdomains and highly defined metal deposition provided catalytic sites for vertical carbon nanotube growth

(CNT).[143] A detailed study on the loading time of precursor (30 seconds to 40 minutes) allowed the researchers to correlate the mean diameter size of Fe_2O_3 nanoparticles to the number of CNTs grown. A work in 2012 by Wu *et al.*[137] demonstrated the true potential of BCP lithography to address ever decreasing technology nodes. The authors reported a method of forming bilayers of cylinder PS-*b*-P2VP structures through controlled swelling conditions. Subsequent Pt metallization of optimized conditions revealed density doubling of both dot and line-space features as shown in Figure 15. The process was also demonstrated using graphoepitaxy schemes.

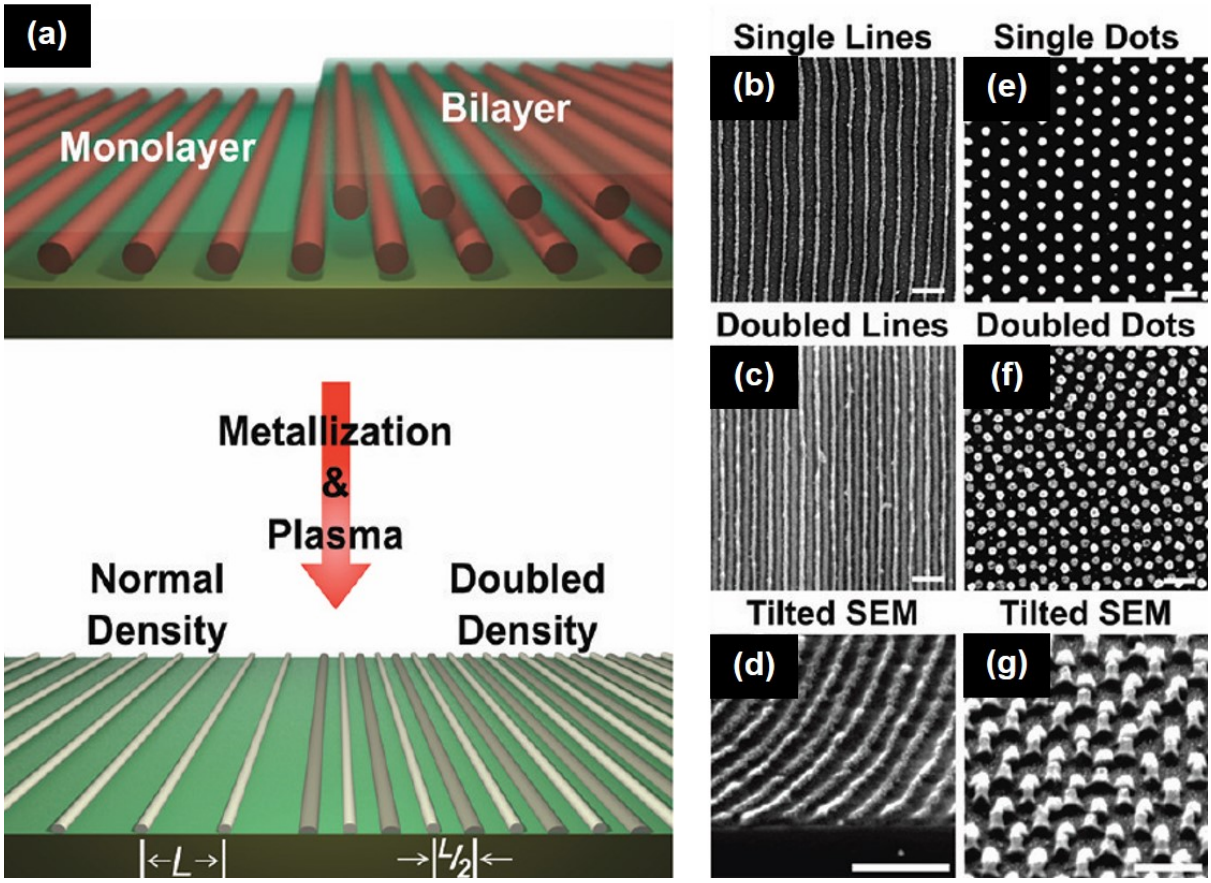


Figure 16. a) Process for density doubling using PS-*b*-P2VP BCP templates. b-g) Resulting density multiplication of Pt features after aqueous metal reduction using bilayer films of PS-*b*-P2VP. All scale bars = 100 nm.

More recent publications by Kim and co-workers[144, 145] have shown sophisticated methods to form highly intricate and technologically relevant materials for catalytic growth and device fabrication. In both reports, PS-*b*-P4VP BCP self-assembly and cylinder orientation (dots or lines) were tuned via solvent vapor annealing and aqueous metal reduction was used to fabricate metallic features. A multi-level charge trap memory device was presented through a Pt-Au binary dot pattern.[144] The Pt-Au binary dot pattern was produced through metallization of vertical cylinder structure that were subsequently used for the self-assembly of a second vertical cylinder layer where metallization was utilized again as shown in **Figure 16**. Additionally, using multicomponent patterns the authors demonstrated the synergy of their features that led to higher extinction over visible and infrared regions. By employing Au nanowire and Pt dots, higher extinction levels were recorded in comparison to either metallic feature alone. The plasmonic capability demonstrated by this work opens many possibilities for light excitation applications.

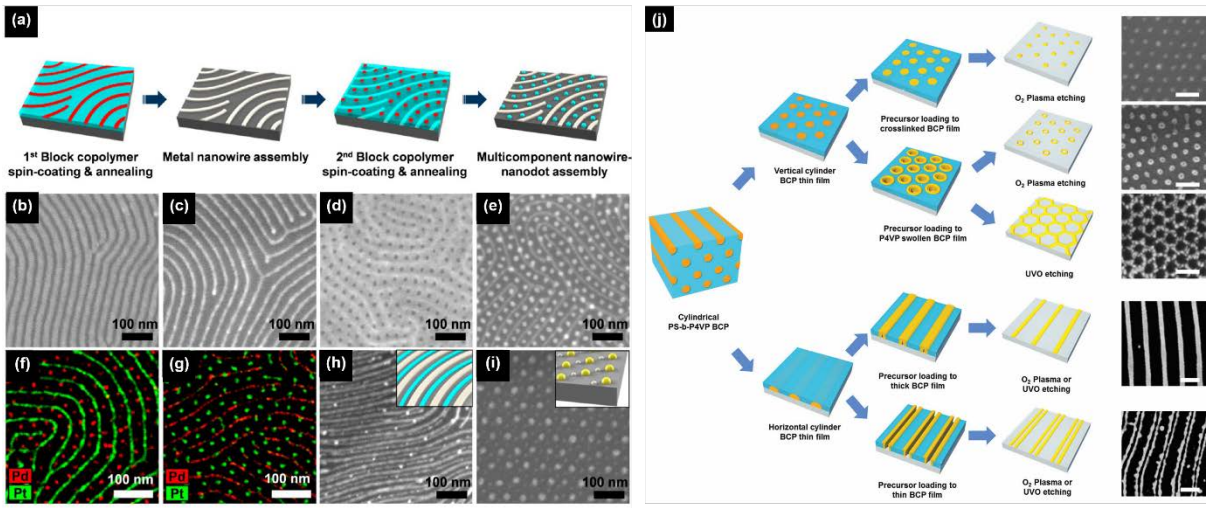


Figure 17. a) Steps involved in multicomponent metallic patterns. b and c) Show SEM images of BCP films and initial Pt nanowire fabrication. d and e) SEM images of BCP nanodot film on Pt metallic lines, followed by Pd dot formation between metallic lines. f and g) EDS elemental mapping of metallic nanodot and nanowire patterns. h and i) SEM images of Pt-Pd nanowire arrays and Au-Pt nanodot arrays. See text for details. i) Schematic summarizing

processes used to fabricate diverse Au patterns from dot and line orientation using a PS-*b*-P4VP BCP template. Top-down SEM images of resulting Au nanostructures are shown. Scale bars = 100 nm.

Note that reports for metallization have used O_2 plasma treatment after metal uptake for removal of polymer matrices to position nanometallic features at substrate surfaces. Thermal annealing, UV/ozone exposure and solution based (*e.g.* selective solvent sonication or short piranha treatments) could also be used effectively to eliminate PS or polymer matrix material. Aqueous metal reduction was also employed to fabricate dimensionally controlled single crystalline intermetallic nanoalloys such as Fe-Co.[145] The synergistic properties enabled accelerated growth of vertical CNTs. The methodology presented highlighted the precision and accuracy that BCP formation coupled with aqueous metal reduction can allow surpassing problematic nucleation, particle agglomeration or growth kinetic issues of other synthetic procedures. In 2015, the methodology was utilized for a cylinder PS-*b*-PEO BCP forming TiO_2 structures for photocatalytic degradation of methylene blue dye.[166] Interestingly, while the infiltration methods in BCPs outlined in previous sections (evaporation/sputtering, ALD, SIS, spin coating methods) have been used for on-chip etch mask function, aqueous metal reduced features have yet to investigated for such purpose. One would assume that the features could be viable for producing high fidelity features upon pattern transfer owing to the robust nature of the metals fabricated. AMR has similar features of metal-salt inclusion described in section 3.4. However, AMR is dictated by chemical interactions that need to be tailored. Metal-salt inclusion largely relies on capillary forces (physical) to replicate BCP templates that have been "activated" and thus may be more useful for a broader range of BCP systems to attain good feature uniformity.

A report by Mun *et al.*[146] has also highlighted the significance of microdomain swelling and its' effect on resulting structures. The authors used PS-*b*-P4VP thin films to create arrays of diverse patterns including Au nanorings, nanomeshes, and double nanowires. Through careful tuning of BCP film thickness, UV/ozone etching, or O_2 plasma treatment structures were transformed from conventional dot and line patterns to the above mentioned diverse features as shown in Figure 16j. The Au patterns were also investigated for their plasmonic properties. The work demonstrated robust patterning processes that can allow the fabrication of intricate metal patterns from simple BCP dot and line patterns.

3.6. Triblock copolymers and inorganic incorporation

A linear tri-BCP is made up of three polymer blocks with a particular block repeated twice (*i.e.* A-B-A), while a tri-BTP consists of three distinct polymer segments covalently bonded together (*i.e.* A-B-C).[167] The generic term "tri-BCP" is used in parts below for simplicity to refer to block polymers composed of three polymer blocks (A-B-A or A-B-C). Note that the terms tri-BCP and tri-BTP are often used interchangeably in the literature.

The bulk of this review has centered on work describing diblock copolymers as these dominate the literature. However more complex systems are receiving interest as they allow more exotic morphologies and arrangements that could have a number of potential applications. Certainly, where more than one "reactive" block exists, there is the possibility of creating complex heterostructures or controlling *e.g.* feature spacing and arrangement beyond simple diblock limitations. Due to the resulting structural variations, tri-BCP features modified via inorganic incorporation techniques outlined in this review may be worth serious consideration to open up diverse nano-applications beyond the scope of work reported hitherto on di-BCP systems. Although work is scarce in this area, it is highly worthwhile assessing the potential of these

systems for creating inorganic material arrangements. Owing to the complexity of tri-BCP features, the potential for sublithographic patterning also deserves attention as recently detailed in an article by de Pablo and co-workers.[168] This section of the review is not comprehensive (reflecting the extent of work), but rather provides the reader with an overview of tri-BCPs ability to form tantalizing structural variations for nanotechnological uses.

Tri-BCPs, both linear and non-linear (star, cyclic) forms can produce dozens of nanoscale architectures with complexity surpassing the basic geometries outlined for di-BCPs (A-B).[169],[170] Tri-BCPs easily allow square packed and core shell cylinder or sphere arrays that are ideal for bit patterned media application.[171] However, the microphase separation of tri-BTPs is also more complex than a simple di-BCP as three χ factors must be considered, *i.e.* $\chi_{AB,}$ $\chi_{BC\ and}$ χ_{CA}. Similarly, three volume fractions contribute to resulting morphologies ($f_a + f_b + f_c = 1$). **Figure 18** displays and outlines some of the exotic morphologies possible via self-assembly of a tri-BTP.[172]

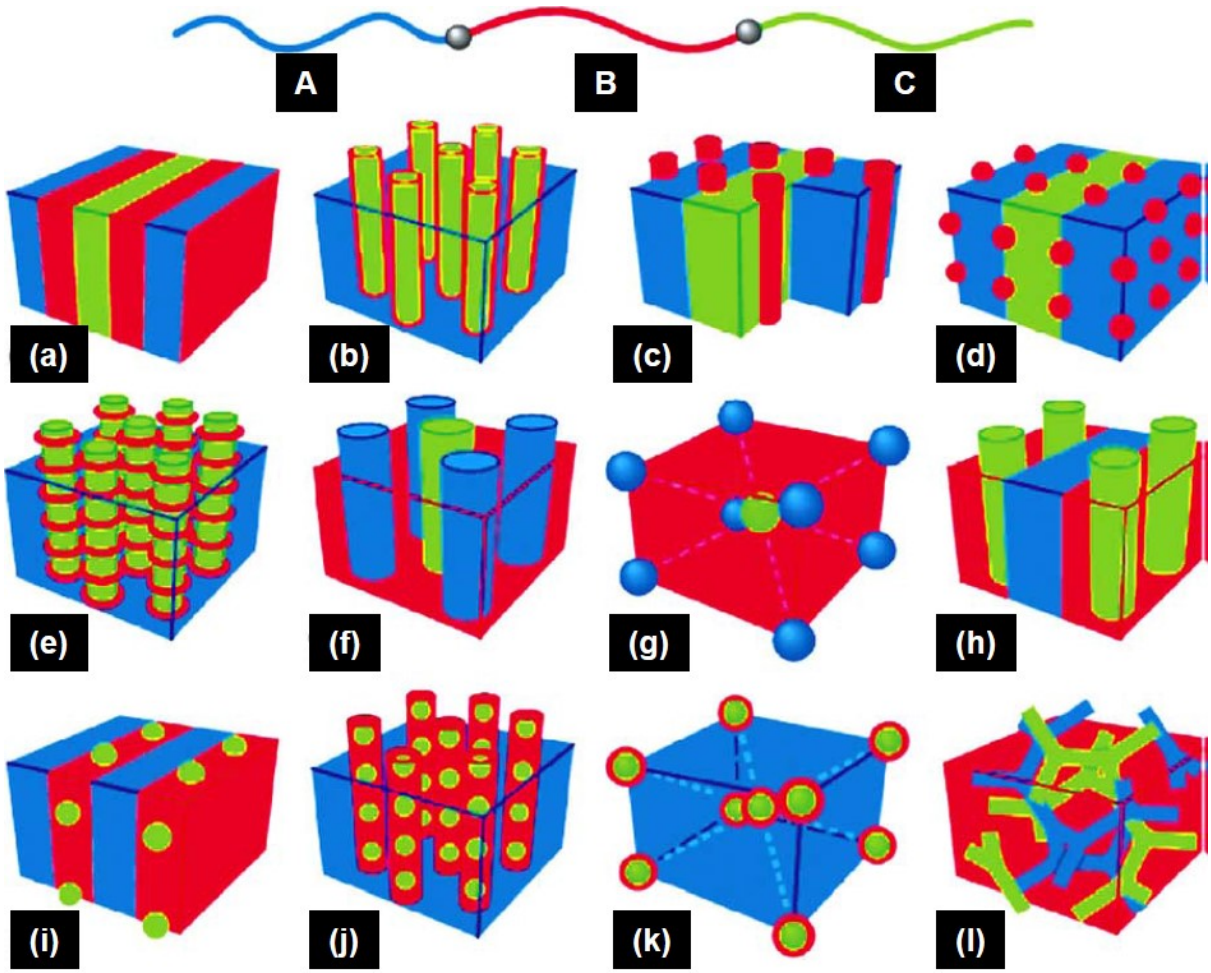


Figure 18. a-l) Schematics show some of the potential morphologies from a tri-block copolymer (A-B-C).

Tri-BTPs share similar governing microphase separation criteria as di-BCPs as morphological structures (and dimensions) are dependent on temperature, block volume fraction and molecular weight. However, the order in which a tri-BTP is arranged (A-B-C or B-A-C or C-A-B) also plays a crucial role in determining the morphological structure.[173]

Tri-BCPs have been well studied as structure directing agents since the early 1990's for mesoporous silica and aluminosilicate templating. Silica and aluminosilicate frames are of particular interest for uses centered on molecular separation, catalysis, and pollution remediation, amongst other functions.[174] In particular, a common industrial class of A-B-A type tri-BCPs under the trade name Pluronic ® (BASF) BCPs have been widely established as

structure directing agents owing to the materials amphiphilic nature in aqueous media. Also referred to as "polaxomers", Pluronic tri-BCPs contain a middle hydrophobic poly(propyleneoxide) block and hydrophilic polyethylene oxide (PEO) blocks at either side, *i.e.* PEO-*b*-PPO-*b*-PEO (see **Figure 19**a). Pluronic's also gained interest for mesoporous material templating[175] as shown in Figure 19b owing to the ability for one to manipulate orientation and chain length and resulting channel size surpassing previous employed practices such as evaporation induced self-assembly (EISA).[176] Key reports by Stucky and co-workers outlined the manipulation of these low-cost surfactants for developing silica fibers with large pore sizes,[177] mesoporous silica,[178] and metal oxide frameworks.[179],[180] Moreover, Pluronic ® BCPs have also been utilized extensively in gene therapy applications,[181],[182] nanomedicine formulations and drug excipients,[183],[184] and thermally responsive gels for protein and peptide delivery.[185] It should be noted that excellent work by the Wiesner, Steiner, and Xu groups have demonstrated the efficacy of BCPs (di- and tri-, as well as supramolecular approaches) and sol-gel chemistry as structure directing agents for functional applications, *e.g.* dye-sensitized solar cells, fuel cells and photonics. The applications will not be discussed in this review and readers are referred to a relevant tutorial and review articles in references [186],[187],[188] and [189].

In more recent reports, evidence of employing tri-BCPs beyond structure directing uses are apparent. Interesting, sophisticated and highly relevant device applicable structures are now evident. An early report from 2003 by Ludwigs *et al.*[190] showed the functional capability of a linear tri-BTP system, PS-*block*-P2VP-*block*-poly(t-butyl methacrylate) (PS-*b*-P2VP-*b*-PtBMA). Following solvent vapor annealing of PS-P2VP-PtBMA thin films, a perforated lamella structure within the thin film was obtained. An impressive degree of order was achieved for hexagonally packed dots as shown in Figure 19d. The chemistry of this tri-BTP provided

added functionality, as the PtBMA could be removed via UV exposure or could be altered through HCl treatment to form poly(methacrylic acid) (PMAA). This report also commented on highly ordered pattern formation irrespective of substrate as confirmed by simulation data. This is an important point as this particular PS-P2VP-PtBMA tri-BCP avoided complex brush modifications unlike those required for di-BCP counterparts, *e.g.* PS-*b*-PMMA[191] or PS-*b*-PDMS[192]. A work by Aizawa *et al.*[193] in 2006 demonstrated the patterning of two metals at substrate surfaces using aqueous metal reduction and a PS-*b*-P2VP-*b*-PEO system, however, ordered uniform patterns were not formed. Also in 2006, a report by Bang *et al.*,[194] demonstrated the possibility of A-B-C tri-BCPs for high density patterning of defect-free porous films with cylinder diameters as small as 10 nm. The work documented the use of PEO-*b*-PMMA-*b*-PS following solvent vapor annealing. As outlined previously in this review, PMMA is extremely susceptible to UV degradation. The midblock of PMMA of PEO-*b*-PMMA-*b*-PS was removed using a brief UV exposure (see Figure 19e). The report was a significant contribution to further extend the work on di-BCP systems. The PEO-*b*-PMMA-*b*-PS tri-BTP effectively surpassed the poor degradability of PS-*b*-PEO BCPs (ethanol exposure has since circumvented this limitation as discussed herein) while extending long range order that is difficult to attain solely with PS-*b*-PMMA BCP systems. Another useful tri-BCP system containing reactive blocks is PI-*b*-PS-*b*-P2VP. In 2011, Lee *et al.*[195] employed PI-*b*-PS-*b*-P2VP to form well-ordered Au nanodots surrounded by a porous silica matrix. After solvent vapor annealing developed well-ordered micellar features (consisting of an outer shell of PI, a middle shell of PS, and a core of P2VP), Au was infused in the P2VP core via immersion in an ethanolic Au precursor solution followed by removal of the PI shell through UV/O_3 to form dense patterns of Au dots. PDMS was spin-coated on the Au patterns and oxygen plasma generated nanoporous silica patterns mimicking the initial PI shell while eliminating the PS shell outside Au dots. This work emphasized the added functionality that tri-BCPs systems can

offer after simple salt immersion and precursor spin-coating techniques are used in combination with reactive tri-BCP systems. Judicious selection of particular reactive tri-BCP systems is essential to allow infiltration and fulfill ones eventual desired nanofeatures. Other tri-BCPs of note include those studied by Epps and co-workers focusing on solvent vapor anneal effects in PdS-*b*-PI-*b*-PdS (d = deuterated) films[196], phase changes due to partial hydrogenation in a PI-*b*-PS-*b*-PMMA system[197], and the precise placement of gold nanoparticle location in well-ordered PS-*b*-PI-*b*-PS patterns[198]. An endless range of architectures are possible beyond di- and tri-BCPs, and recently multiblocks have been suggested to open a “Pandora’s box” of design space by virtue of synthetic polymer advances.[199]

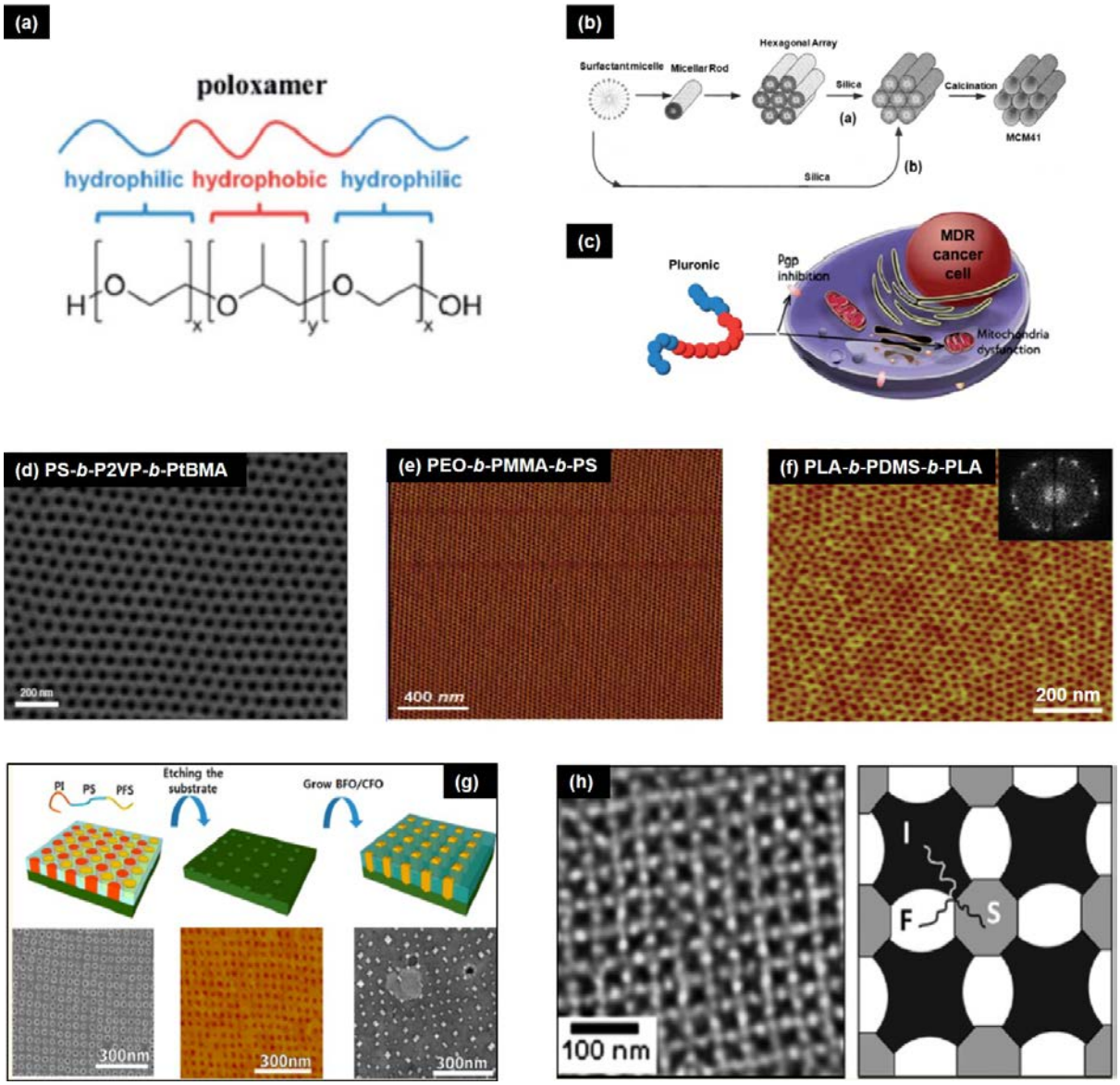


Figure 19. a) Chemical structure of PEO-*b*-PPO-*b*-PEO tri-BCP. See text for further details. b) Synthesis route using Pluronic species for inorganic framework. c) Bio-application of Pluronic BCP for nanomedicine. Well defined nanodot patterns from d) PS-*b*-P2VP-*b*-PtBMA, e) PEO-*b*-PMMA-*b*-PS, f) and PLA-*b*-PDMS-*b*-PLA. g) Multiferroic composite growth based on PI-*b*-PS-*b*-PFS, see text for details. h) SEM image of Archimedean tiling pattern formed through a miktoarm star terpolymer PI-arm-PS-arm-PFS and schematic representation.

Publications by Hillmyer and co-workers have illustrated the potential functional capacity of PLA containing tri-BCPs with examples for nanolithographic application (using PLA-*b*-

PDMS-*b*-PLA[200] - see Figure 19f, and PS-*b*-PI-*b*-PLA[201]) ultrafiltration membranes (using PS-*b*-PI-*b*-PLA[202]), porous linear polyethylene channels (using PLA-*b*-LPE-*b*-PLA[203]), and poly(acrylic acid) coated PS channels (using PS-*b*-PDMA-*b*-PLA[204]). The molecular design routes generated added functionality to basic polymer blocks that can possibly address various membrane and separation science technological challenges. Additionally, the BCPs developed with rapidly degradable PLA components combined with the incorporation methods outlined in this review could lead to intricate hybrid materials for alternative device uses.

Likewise, Manners, Ross, and co-workers have explored tri-BTPs and miktoarm polymers for etch mask applications and functional use. In 2009, the synthesis and self-assembly of a new tri-BTP was described for developing nanoscale ring patterns.[205] After solvent vapor annealing of a PS-*b*-poly(ferrocenylsilane)-*b*-P2VP (PS-*b*-PFS-*b*-P2VP) BTP, a PS core and PFS shell in a P2VP matrix was developed. PFS, an iron and silicon containing moiety, is particularly useful as a BCP component due to its resistance to dry etching as detailed earlier. The authors reported the use of PS and P2VP etched films forming robust PFS ring arrays that were subsequently used as lithographic templates for transferring to a PS polymer layer via imprinting. Another work involving a PFS containing tri-BTP, PI-*b*-PS-*b*-PFS, was employed for patterning pits in a Nb-doped $SrTiO_3$ substrate.[206] These square symmetry pits (period = 44 nm) were utilized for nanocomposite growth and fabrication of multiferroic $BiFeO_3$-$CoFe_2O_4$ material (see Figure 19g). The PI-*b*-PS-*b*-PFS system has also been demonstrated forming square arrays of dot and hole patterns along with combinations of both.[207] More exotic BCP materials including a miktoarm star terpolymer PI-arm-PS-arm-PFS blended with a homopolymer have been explored for patterning Archimedean tilings (see Figure 19h) for nanolithographic application and DSA application.[208],[209] The works illustrated a gallery of

fascinating structural variations which could potentially be used beyond etch mask applications.

Many of the tri-BCP systems mentioned above contain a reactive block like PEO, PI and PVP, or an easily etched block such as PMMA or PLA, all of which can be infiltrated. Such desirable chemical attributes in tri-BCP systems further the potential to access bimetallic or trimetallic hybrid systems using innovative incorporation techniques. Additionally, metal containing BCPs like PFS systems could easily be altered post self-assembly to add another metal component. Thus far, works on such systems to incorporate further inorganic material are scarce and could enable multi-functionality beyond simple di-BCP arrays.

3.7. Challenges and Emerging Applications

3.7.1. Extending incorporation methods to ultra-low BCP nanodimensions

Whilst excellent work has been reported for insertion of inorganics into BCP nanopatterns and effective pattern transfer, further work is required to scale these processes to the deep nanoscale regime for nanolithography application. The library of "high χ" BCPs that exist will potentially facilitate nanopatterns with sub-16 nm periods. The existence of a more defined block-block interface in "high χ" BCPs (as interfacial width of BCP microdomains are proportional to $\chi^{-0.5}$) [210] should also enable the creation of desired uniform features acceptable for IC designs. Moreover, "high χ" materials will allow processes to meet accepted values for line edge roughness and resolution (and throughput), a triad also known as the lithographic "triangle of death".[211],[212] With an inherently more defined block-block interface, incorporation methods will allow successful pattern transfer to the underlying substrate. In this regard, SIS processes focusing on PS-*b*-PMMA will struggle to define sub-20 nm periods and modified PS-*b*-PMMA BCPs may have to be evaluated. Furthermore, evaporation or sputtering methods may also be

hindered in achieving feature uniformity due to the ultra-low nanodimensions involved (sub-20 nm periods and sub-10 nm feature sizes) and eventual lift-off or Damascene-like processes will damage deposited material.

It is foreseeable that ultra-low nanoscale patterning of features that can be pattern transferred or used for functional use will be enabled via routes encompassing design and manipulation of well-defined reactive sites in polymer components as well as tailored selective chemistry mediating polymer and precursor interactions. Such processes will have to be optimized to realize large scale fabrication of inorganic nanofeatures with one to one registration of the initial BCP pattern. For example, direct bonding sites in BCP components (like PVPs) will allow a more site specific registration of an inorganic precursor in comparison to physical incorporation processes like evaporation and sputtering. ALD processes coupled with careful BCP selection may also become more prevalent for pushing scaling limits owing to the extreme precision in deposited layers and the associated self-limiting reactions at reactive sites. Moreover, while reservations on "in-situ" inclusion methods were outlined in the introduction, it is possible that such routes or "doping" via metal chelation may be the only viable route to enable ultrasmall BCP dimensions. Metal chelation of BCP species is well-known to increase the effective interaction parameter (χ_{eff}),[213] and most reports so far suggest that a linear relationship exists between increasing χ_{eff} and higher salt concentration loading.[214] For example, "doping" of lamellar PS-*b*-PEO[215] and P2VP-*b*-PS-*b*-P2VP[216] BCPs has been exploited recently through complexing lithium (in PEO microdomains) and copper (in P2VP microdomains) ions for accessing 16 nm and 14 nm periods respectively (see **Figure 20**a-c). However, careful tuning is essential with such methods to avoid micellization. In conjunction with salt additions to BCPs, sugar based BCPs[217],[218],[219] may become more prevalent for nanoscale patterning owing to the enhanced chemical dissimilarity (*i.e.* high χ) of saccharidic

and synthetic blocks allowing low periods and feature sizes to accessed. Since sugar based blocks can contain a number of oxygen's, dry etching should allow their facile removal and the inclusion and design of well-defined inorganic templates utilizing incorporation methods.

It is worth noting the emergence of BCPs with feature and periods exceeding 100 nm and their potential applicability. Various reports on large BCP features are now evident and may present an ideal route to fabricating metamaterials and photonic structures.[220] Reports have detailed the self-assembly of large periods using large molecular weight (> 1 million g mol^{-1}) BCPs[221] and brush-type BCPs[222],[223]. A recent review[224] has also highlighted this emerging area of patterning large period features from such polymer materials. Whilst such macromolecules allow for interesting fundamental studies due to their enhanced side chain mobility allowing microphase separation, incorporating inorganic material using methods detailed in this review could lead to a diverse range of light active materials. The incorporation process in such large scale features should be facile in comparison to sub-50 nm BCP microdomains. This would provide a low cost route to well-defined inorganic features or pattern transferred nanostructures for polarizers and other photonic bandgap applications.

3.7.2. Metrology and incorporation techniques

The existence and characterization of defects in BCP polymer films has begun to emerge as an area where inorganic infiltration may contribute significantly to (i) identifying defects within the plane of the film and (ii) understanding defect evolution. While defects at the top surface (*i.e.* polymer/air interface) have always been routinely characterized via AFM or SEM, "hidden" defects within the plane of the film may exist that one cannot observe. Unidentified defects within a film may only become apparent on pattern transfer and thus elucidating such features is critical for device application and function. Current SEM tools and practices of

identifying BCP features may not fully recognize surface defects and may be more suitably characterized in the future by Helium Ion Microscopy (HIM) due to the its' superior resolution.[225] Lately, a range of methods have been reported for identifying in-plane defects through 3-D metrology methods. For example, Sunday *et al*.[226],[227] reported a technique using resonant critical dimension small angle x-ray scattering (res-CDSAXS) to three-dimensionally characterize buried features of PS-*b*-PMMA lamellar films in DSA schemes. The methodology has also been utilized to examine pattern transfer of a Cr-evaporated mask versus SIS infused features of a lamellar forming PS-*b*-PMMA BCP.[228] The scattering technique elucidated periodic variations due to the shape or spacing of patterning transferred silicon features using the SIS etch mask. It was speculated that the SIS infusion method is the primary contributing issue to such issues since neither the Cr nor PS line patterns displayed comparable variations. The SIS process has also recently been used to identify and characterize defects (see Figure 20d) within the plane of a BCP film, *i.e.* in 3-D. Nealey and co-workers[229] have used scanning transmission electron microscopy (STEM) tomography to investigate SIS infused PMMA features in spherical, cylindrical and lamellar forming PS-*b*-PMMA films. The selective incorporation of an inorganic phase allows facile interpretation of defects using STEM tomography. The authors also noted how the SIS process was tuned to minimize any potential swelling of features that may distort interpretation. The technique bypasses any issues that may result from staining or etching of domains that can create further defects. The methodology also allows the identification of individual defects which is not possible using res-CDSAXS studies. TEM tomography has previously been employed to study bilayer PS-*b*-PDMS films since PDMS possesses sufficient block mass contrast for bright field imaging.[230] However, the SIS procedure now allows analyses of BCP defects and similar in 3-D's in PS-*b*-PMMA BCPs. The process could be extremely effective for characterizing a whole host of commonly examined BCP systems that do not inherently hold sufficient phase contrast. This also opens

up an interesting platform whereby simple methods using volatile selective vapors selectively infuse into BCP features could be analysed using STEM tomography. Moreover, while STEM tomography provides fundamental insight into the nature of defect structures, SIS infused features may allow for GISAXS experiments to assess global coverage.

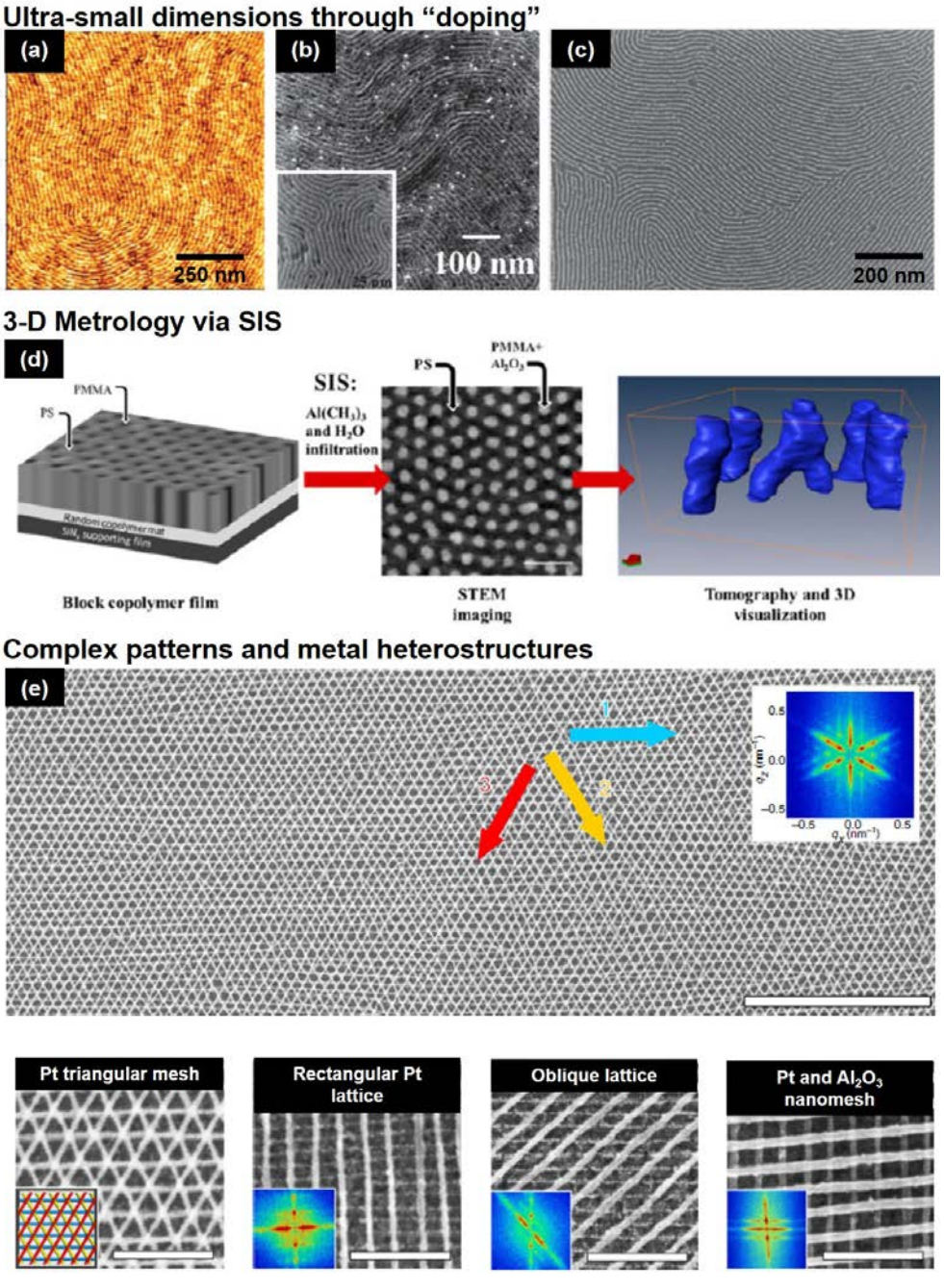


Figure 20. a,b) AFM and SEM images of lithium chloride doped lamellar PS-*b*-PEO microphase separated films with 16 nm period. c) SEM image of Pt nanowires with a 14.1 nm period formed using aqueous metal reduction of a copper chloride doped P2VP-*b*-PS-*b*-P2VP

lamellar system. d) Process for identifying and assessing individual defects in PS-*b*-PMMA BCP films using Sequential Infiltration Synthesis and Scanning Transmission Electron Tomography. e) Top-down SEM image of a three-layered hexagonal lattice via soft-shear laser zone annealing of PS-*b*-P2VP films. Scale bar = 1 micron. SEM images below show other intricate patterns attainable and heterostructures. Scale bars for bottom SEM images = 200 nm.

3.7.3. Complex pattern and heterostructure formation

The formation of complex and intricate patterns has lately emerged for some interesting device applications as described earlier. A recent progress report[231] has also outlined BCP patterning applications in relation to electronic devices, electronic sensors, and energy devices. However, focus on the design and manipulation of next-generation BCP patterning for complex patterns was not discussed. As emphasized earlier, tri-BCPs deserve further exploration for device patterning and inclusion of inorganic moieties. However, researchers are still pushing the limits of di-BCPs via different annealing and incorporation processes to show unique hybrid pattern formations. Recently, Yager and co-workers[232] demonstrated a host of symmetries using a simple di-BCP, PS-*b*-P2VP. BCP patterns and their inorganic replicas were formed demonstrated lines, squares, rhombuses, rectangles, parallelograms and triangles. For example, to create triangle arrays, a monolayer PS-*b*-P2VP film was aligned using soft-shear laser zone annealed (SS-LZA) to form line features. This initial line features were converted into Pt wires using the aqueous metal reduction process. A successive line pattern was then aligned in a different axis to the underlying metal feature followed by a final third overlayer producing aligned features in a different axis. In order to create rectangular lattices or parallelograms, two different BCP molecular weights were required. It is evident that the method employed by the authors allows heterostructures to be attained very easily. Pt nanowires were developed using the aqueous metal reduction process while an additional BCP overlayer was infused via the

SIS process to create an Al_2O_3 nanowire. ZnO semiconductor features along with other metallic features and morphologies were also shown. One should note a work reported (prior to the above SS-LZA process) by Register and co-workers[233] that also developed inorganic nanomesh and nanosquare arrays using soft-shear alignment with a metal containing di-BCP. These works have illustrated simple processes to fabricate complex features not routinely accessible for simple di-BCP monolayer films. Attempting to access unconventional morphologies could lead to new and exciting exploits in this polymer science area that allows low-cost, reproducible and an industrial scalable technology. Such processes, morphologies and dimensions are not routinely attained using expensive "top-down" lithography tools.

While the above highlighted examples have introduced complex pattern formation from multiple layers of BCP thin films, other researchers have pushed the boundaries with respect to pattern formation from di-BCP systems using BCP blends. For example, excellent work has been reported recently by Park *et al.*[234],[235] where ring shaped phase changed memory structures have been fabricated via blending of di-BCP systems and metal evaporation. PDMS-*b*-PS and PS-PFS BCP blends were optimized to form dot-in-hole nanocomposites on $Ge_2Sb_2Te_5$/TiN/(Ti)W/SiO_2/Si substrates. Pt evaporation was to generate nanoring patterns acting as etch masks to pattern $Ge_2Sb_2Te_5$ nanoring features that exhibited low switching currents. Such creative paths represent a new direction for more complex heterostructure formation that could possibly be tuned to incorporate more exotic infiltrated species when using reactive blended BCPs, e.g. PS-*b*-PFS and PS-*b*-PxVPs.

Heterostructure formation could allow the BCP field to address more diverse challenges and applications in the sensor, biomedical and energy fields. For example, future portable devices are expected to possess more functionality. One could utilize complex BCP nanopatterns to

incorporate photoactive or energy harvesting inorganic nanomaterial for a “zero power” component of a portable smart device. “Zero power” technologies are ones that can generate or harvest their energy from their immediate surroundings, *e.g.* light, heat, electromagnetic radiation, *etc*. Such technologies are important considering the world’s ever-increasing energy use. Both the high areal density and complex heterostructure features that can be developed via BCP patterning and inorganic insertion may provide a promising platform for future charge storage devices.

3.8. Conclusions

Microphase separated BCP films are well-established templates for pattern formation at the nanoscale and have been studied as potential on-chip etch masks for next-generation electronic devices. They have matured to a stage where semiconductor integration is actively being assessed through pilot schemes.[236],[237],[238] Such steps forward illustrate the level of understanding and strong efforts that the DSA/BCP discipline has received in the past decade. Likewise, DSA/BCP patterning is a very promising candidate for bit patterned media beyond 1 Tb in^{-2} as initial investment and operating costs are extremely low in comparison to methods such as photolithography, electron-beam lithography or nanoimprint lithography.[239],[240]While fundamental study has always been prominent in this macromolecular area, multi-disciplinary academic and industrial efforts focusing on applied areas have also aided in reaching exquisite nanoscale BCP features. Moreover, new exciting reports on BCP functionality beyond basic patterns are now evident.

We have highlighted recent reports that have emerged on BCP film formation for incorporating inorganic material for on-chip etch mask and other functional use. Importantly, the densities and coverages accessible with BCP templates make them a unique self-assembling material for

device fabrication. Whilst many milestones have been achieved, the work to realize non-electronic applications is very much in its' infancy and thus provides scope for further improvement and discovery.

Evaporation and sputtering methods outlined in section 3.1. have proven quite fruitful for proof of concept in early work on the positional accuracy and manipulation of inorganic material on slight modifications (minor block etching, swelling) of neat BCP templates. It appears that evaporation (thermal or e-beam) and radio frequency sputtering are quite amenable to BCP templates and industrial fabrication processes as high temperatures are not necessary limiting potential damage to BCP morphologies or device performance issues.

The successive sections largely detailed more recent reports of inorganic inclusion at the nanoscale utilizing BCPs. Many approaches have been employed illustrating the diverse nature and ability of BCPs to incorporate functional material after self-assembly. Interestingly, growth sites (via sequential infiltration synthesis), "activation" (metal-salt inclusion), and acidic media (aqueous metal reduction) have been employed as ways to enhance uptake and overall uniformity for inorganic inclusion. Pattern transfer of high fidelity structures has not been demonstrated with evaporation/sputtering or aqueous metal reduction methods. In contrast, ALD, SIS and metal-salt inclusion practices provide routes for reproducibly generating high-fidelity nanostructures for on-chip etch mask application and therefore one would assume will lead the way for device patterning and integration in the deep nanoscale regime.

The deeper understanding of BCP self-assembly has led to many improvements where microdomains can be dictated and aligned over large scale areas. In the more recent studies (< 5 years) discussed above, one observes a distinct enhancement in BCP ordering and orientation

using higher χ BCP materials such as PS-*b*-PxVP (x = 2 or 4), PS-*b*-PDMS and PS-*b*-PLA compared to the low χ PS-*b*-PMMA. BCP nanopattern improvements are primarily related to high χ factor as line edge roughness is reduced and microphase separation is more likely to occur. Additionally, knowledge of influencing BCP environmental and processing conditions is continually evolving and more sophisticated annealing protocols are being implemented achieving ultra-fast processing periods (sub-1 minute)[45],[241],[42],[46],[242],[243],[244],[245],[246],[247] whilst still retaining superb pattern ordering. Such milestones on BCP control coupled with inorganic infiltration techniques only further enhance the viability of BCP nanopatterning for application in electronic and non-electronic based technologies.

ACKNOWLEDGMENT

Funding Sources: The authors gratefully acknowledge Science Foundation Ireland (SFI) (Grant number 09/IN.1/602) grant for funding this project.

3.9. References

[1] R. A. Farrell, T. G. Fitzgerald, D. Borah, J. D. Holmes, M. A. Morris, International Journal of Molecular Sciences 2009, 10, 3671.
[2] N. Hadjichristidis, M. Pitsikalis, H. Iatrou, in *Block Copolymers I*, Vol. 189 (Ed: V. Abetz), 2005, 1.
[3] H. Arslan, *Block and Graft Copolymerization by Controlled/Living Radical Polymerization Methods*, 2012.
[4] D. J. Keddie, Chemical Society Reviews 2014, 43, 496.
[5] F. S. Bates, G. H. Fredrickson, Annual Review of Physical Chemistry 1990, 41, 525.
[6] M. J. Fasolka, A. M. Mayes, Annual Review of Materials Science 2001, 31, 323.
[7] I. W. Hamley, Nanotechnology 2003, 14, R39.
[8] M. P. Stoykovich, P. F. Nealey, Materials Today 2006, 9, 20.
[9] M. Li, C. K. Ober, Materials Today 2006, 9, 30.
[10] S. Krishnamoorthy, C. Hinderling, H. Heinzelmann, Materials Today 2006, 9, 40.
[11] I. W. Hamley, Progress in Polymer Science 2009, 34, 1161.
[12] J. Bang, U. Jeong, D. Y. Ryu, T. P. Russell, C. J Hawker, Advanced Materials 2009, 21, 4769.
[13] J. N. L. Albert, T. H. Epps III, Materials Today 2010, 13, 24.
[14] H. C. Kim, S. M. Park, W. D. Hinsberg, I. R. Division, Chemical Reviews 2010, 110, 146.

[15] J. K. Kim, S. Y. Yang, Y. Lee, Y. Kim, Progress in Polymer Science 2010, 35, 1325.
[16] F. H. Schacher, P. A. Rupar, I. Manners, Angewandte Chemie - International Edition 2012, 51, 7898.
[17] B. H. Kim, J. Y. Kim, S. O. Kim, Soft Matter 2013, 9, 2780.
[18] M. Luo, T. H. Epps, Macromolecules 2013, 46, 7567.
[19] H. Hu, M. Gopinadhan, C. O. Osuji, Soft Matter 2014, 10, 3867.
[20] I. Botiz, S. B. Darling, Materials Today 2010, 13, 42.
[21] C. Park, J. Yoon, E. L. Thomas, Polymer 2003, 44, 6725.
[22] T. P. Lodge, Macromolecular Chemistry and Physics 2003, 204, 265.
[23] R. A. Segalman, Materials Science & Engineering R-Reports 2005, 48, 191.
[24] S. E. Thompson, S. Parthasarathy, Materials Today 2006, 9, 20.
[25] C. J. Hawker, T. P. Russell, MRS Bulletin 2005, 30, 952.
[26] S. B. Darling, Progress in Polymer Science 2007, 32, 1152.
[27] C. A. Ross, J. Y. Cheng, MRS Bulletin 2008, 33, 838.
[28] S.-J. Jeong, J. Y. Kim, B. H. Kim, H.-S. Moon, S. O. Kim, Materials Today 2013, 16, 468.
[29] M. A. Morris, Microelectronic Engineering 2015, 132, 207.
[30] G. E. Moore, Electronics 1965, 38, 114.
[31] H. Tsai, J. W. Pitera, H. Miyazoe, S. Bangsaruntip, S. U. Engelmann, C.-C. Liu, J. Y. Cheng, J. J. Bucchignano, D. P. Klaus, E. A. Joseph, D. P. Sanders, M. E. Colburn, M. A. Guillorn, ACS Nano 2014, 8, 5227.
[32] S.-J. Jeong, S. O. Kim, Journal of Materials Chemistry 2011, 21, 5856.
[33] M. P. Stoykovich, M. Müller, S. O. Kim, H. H. Solak, E. W. Edwards, J. J. De Pablo, P. F. Nealey, Science 2005, 308, 1442.
[34] R. Ruiz, H. Kang, F. A. Detcheverry, E. Dobisz, D. S. Kercher, T. R. Albrecht, J. J. de Pablo, P. F. Nealey, Science 2008, 321, 936.
[35] C. T. Black, ACS Nano 2007, 1, 147.
[36] X. Gu, I. Gunkel, T. P. Russell, Philosophical Transactions of the Royal Society A: Mathematical, Physical and Engineering Sciences 2013, 371.
[37] M. Ramanathan, Y.-C. Tseng, K. Ariga, S. B. Darling, Journal of Materials Chemistry C 2013, 1, 2080.
[38] A. Nunns, J. Gwyther, I. Manners, Polymer 2013, 54, 1269.
[39] Y. Mai, A. Eisenberg, Chemical Society Reviews 2012, 41, 5969.
[40] C. Sinturel, M. Vayer, M. Morris, M. A. Hillmyer, Macromolecules 2013, 46, 5399.
[41] C. M. Bates, M. J. Maher, D. W. Janes, C. J. Ellison, C. G. Willson, Macromolecules 2013, 47, 2.
[42] W. I. Park, K. Kim, H.-I. Jang, J. W. Jeong, J. M. Kim, J. Choi, J. H. Park, Y. S. Jung, Small 2012, 8, 3762.
[43] K. W. Gotrik, C. A. Ross, Nano Letters 2013, 13, 5117.
[44] D. E. Angelescu, J. H. Waller, D. H. Adamson, P. Deshpande, S. Y. Chou, R. A. Register, P. M. Chaikin, Advanced Materials 2004, 16, 1736.
[45] X. Zhang, K. D. Harris, N. L. Y. Wu, J. N. Murphy, J. M. Buriak, ACS Nano 2010, 4, 7021.
[46] W. I. Park, J. M. Kim, J. W. Jeong, Y. S. Jung, ACS Nano 2014, 8, 10009.
[47] C. A. Ross, K. K. Berggren, J. Y. Cheng, Y. S. Jung, J.-B. Chang, Advanced Materials 2014, 26, 4386.
[48] W. M. Moreau, Plenum Publishing Corp 1988.
[49] M. Park, P. M. Chaikin, R. A. Register, D. H. Adamson, Applied Physics Letters 2001, 79, 257.
[50] M. Park, C. Harrison, P. M. Chaikin, R. A. Register, D. H. Adamson, Science 1997, 276, 1401.
[51] P. Mansky, P. Chaikin, E. L. Thomas, Journal of Materials Science 1995, 30, 1987.
[52] P. Mansky, C. K. Harrison, P. M. Chaikin, R. A. Register, N. Yao, Applied Physics Letters 1996, 68, 2586.
[53] K. W. Guarini, C. T. Black, K. R. Milkove, R. L. Sandstrom, Journal of Vacuum Science & Technology B 2001, 19, 2784.

[54] C. T. Black, K. W. Guarini, K. R. Milkove, S. M. Baker, T. P. Russell, M. T. Tuominen, Applied Physics Letters 2001, 79, 409.
[55] K. Shin, K. A. Leach, J. T. Goldbach, D. H. Kim, J. Y. Jho, M. Tuominen, C. J. Hawker, T. P. Russell, Nano Letters 2002, 2, 933.
[56] R. A. Farrell, N. Petkov, M. T. Shaw, V. Djara, J. D. Holmes, M. A. Morris, Macromolecules 2010, 43, 8651.
[57] D. Borah, M. T. Shaw, S. Rasappa, R. A. Farrell, C. O. Mahony, C. M. Faulkner, M. Bosea, P. Gleeson, J. D. Holmes, M. A. Morris, Journal of Physics D: Applied Physics 2011, 44, 174012.
[58] S. G. Xiao, X. M. Yang, E. W. Edwards, Y. H. La, P. F. Nealey, Nanotechnology 2005, 16, S324.
[59] V. Gowrishankar, N. Miller, M. D. McGehee, M. J. Misner, D. Y. Ryu, T. P. Russell, E. Drockenmuller, C. J. Hawker, Thin Solid Films 2006, 513, 289.
[60] Z. Danilo, K. Dong Ha, P. M. Alexey, H. Sigrid, S. Roland, G. Petra, H. Reinald, S. Stephan, J. H. Craig, P. R. Thomas, S. Martin, G. Ulrich, Nanotechnology 2006, 17, 2122.
[61] K. S. Deepak, V. K. Robert, X. Hongqi, X. Ting, P. R. Thomas, T. T. Mark, Nanotechnology 2008, 19, 245305.
[62] S. Park, B. Kim, A. Cirpan, T. P. Russell, Small 2009, 5, 1343.
[63] D. H. Lee, D. O. Shin, W. J. Lee, S. O. Kim, Advanced Materials 2008, 20, 2480.
[64] S.-J. Jeong, J. E. Kim, H.-S. Moon, B. H. Kim, S. M. Kim, J. B. Kim, S. O. Kim, Nano Letters 2009, 9, 2300.
[65] S.-J. Jeong, H.-S. Moon, J. Shin, B. H. Kim, D. O. Shin, J. Y. Kim, Y.-H. Lee, J. U. Kim, S. O. Kim, Nano Letters 2010, 10, 3500.
[66] J. W. Choi, M. Kim, N. S. Safron, M. S. Arnold, P. Gopalan, ACS Applied Materials & Interfaces 2014, 6, 9442.
[67] P. Pellegrino, M. Perego, S. Schamm-Chardon, G. Seguini, A. Andreozzi, F. F. Lupi, C. Castro, G. B. Assayag, physica status solidi (a) 2013, 210, 1477.
[68] S. Rasappa, D. Borah, R. Senthamaraikannan, C. C. Faulkner, J. J. Wang, J. D. Holmes, M. A. Morris, Science of Advanced Materials 2013, 5, 782.
[69] T. Thurn-Albrecht, J. Schotter, G. A. Kästle, N. Emley, T. Shibauchi, L. Krusin-Elbaum, K. Guarini, C. T. Black, M. T. Tuominen, T. P. Russell, Science 2000, 290, 2126.
[70] S. B. Darling, A. Hoffmann, Journal of Vacuum Science & Technology A 2007, 25, 1048.
[71] M. Kreuzer, C. Simão, A. Diaz, C. M. Sotomayor Torres, Macromolecules 2014, 47, 8691.
[72] S. Park, J.-Y. Wang, B. Kim, T. P. Russell, Nano Letters 2008, 8, 1667.
[73] A. J. Hong, C.-C. Liu, Y. Wang, J. Kim, F. Xiu, S. Ji, J. Zou, P. F. Nealey, K. L. Wang, Nano Letters 2010, 10, 224.
[74] A. Baruth, M. Seo, C. H. Lin, K. Walster, A. Shankar, M. A. Hillmyer, C. Leighton, ACS Applied Materials & Interfaces 2014.
[75] X. Gu, P. Dorsey, T. P. Russell, Advanced Materials 2012, 24, 5505.
[76] J. G. Son, K. W. Gotrik, C. A. Ross, ACS Macro Letters 2012, 1, 1279.
[77] M. Huda, J. Liu, Y. Yin, S. Hosaka, Japanese Journal of Applied Physics 2012, 51.
[78] W. Gu, J. Xu, J.-K. Kim, S. W. Hong, X. Wei, X. Yang, K. Y. Lee, D. S. Kuo, S. Xiao, T. P. Russell, Advanced Materials 2013, 25, 3677.
[79] S. Hosaka, T. Akahane, M. Huda, H. Zhang, Y. Yin, ACS Applied Materials & Interfaces 2014.
[80] D. Kim, S.-B. Jeon, J. Y. Kim, M.-L. Seol, S. O. Kim, Y.-K. Choi, Nano Energy 2015, 12, 331.
[81] C. K. Jeong, K. M. Baek, S. Niu, T. W. Nam, Y. H. Hur, D. Y. Park, G.-T. Hwang, M. Byun, Z. L. Wang, Y. S. Jung, K. J. Lee, Nano Letters 2014, 14, 7031.
[82] Y. S. Jung, W. Jung, H. L. Tuller, C. A. Ross, Nano Letters 2008, 8, 3776.
[83] W. I. Park, J. M. Yoon, M. Park, J. Lee, S. K. Kim, J. W. Jeong, K. Kim, H. Y. Jeong, S. Jeon, K. S. No, J. Y. Lee, Y. S. Jung, Nano Letters 2012, 12, 1235.
[84] J. Lee, K. Kim, W. I. Park, B.-H. Kim, J. H. Park, T.-H. Kim, S. Bong, C.-H. Kim, G. Chae, M. Jun, Y. Hwang, Y. S. Jung, S. Jeon, Nano Letters 2012, 12, 6078.

[85] J. Frascaroli, S. Brivio, F. Ferrarese Lupi, G. Seguini, L. Boarino, M. Perego, S. Spiga, ACS Nano 2015, 9, 2518.
[86] Y. S. Jung, J. H. Lee, J. Y. Lee, C. A. Ross, Nano Letters 2010, 10, 3722.
[87] Y. S. Jung, J. B. Chang, E. Verploegen, K. K. Berggren, C. A. Ross, Nano Letters 2010, 10, 1000.
[88] Y. S. Jung, W. Jung, C. A. Ross, Nano Letters 2008, 8, 2975.
[89] Y. S. Jung, C. A. Ross, Small 2009, 5, 1654.
[90] A. Baruth, M. D. Rodwogin, A. Shankar, M. J. Erickson, M. A. Hillmyer, C. Leighton, ACS Applied Materials & Interfaces 2011, 3, 3472.
[91] A. J. M. Mackus, A. A. Bol, W. M. M. Kessels, Nanoscale 2014, 6, 10941.
[92] V. Suresh, M. S. Huang, M. P. Srinivasan, S. Krishnamoorthy, ACS Applied Materials & Interfaces 2013, 5, 5727.
[93] Y. Wang, Y. Qin, A. Berger, E. Yau, C. He, L. Zhang, U. Gösele, M. Knez, M. Steinhart, Advanced Materials 2009, 21, 2763.
[94] H.-S. Moon, J. Y. Kim, H. M. Jin, W. J. Lee, H. J. Choi, J. H. Mun, Y. J. Choi, S. K. Cha, S. H. Kwon, S. O. Kim, Advanced Functional Materials 2014, 24, 4343.
[95] G. Gay, T. Baron, C. Agraffeil, B. Salhi, T. Chevolleau, G. Cunge, H. Grampeix, J. H. Tortai, F. Martin, E. Jalaguier, B. D. Salvo, Nanotechnology 2010, 21, 435301.
[96] S. Tallegas, T. Baron, G. Gay, C. Aggrafeil, B. Salhi, T. Chevolleau, G. Cunge, A. Bsiesy, R. Tiron, X. Chevalier, C. Navarro, K. Aissou, I. Otsuka, S. Halila, S. Fort, R. Borsali, physica status solidi (c) 2013, 10, 1195.
[97] C. Hägglund, G. Zeltzer, R. Ruiz, I. Thomann, H.-B.-R. Lee, M. L. Brongersma, S. F. Bent, Nano Letters 2013, 13, 3352.
[98] J. Yin, X. Yao, J.-Y. Liou, W. Sun, Y.-S. Sun, Y. Wang, ACS Nano 2013, 7, 9961.
[99] J. Yang, L. Tong, Y. Yang, X. Chen, J. Huang, R. Chen, Y. Wang, Journal of Materials Chemistry C 2013, 1, 5133.
[100] F. Li, X. Yao, Z. Wang, W. Xing, W. Jin, J. Huang, Y. Wang, Nano Letters 2012, 12, 5033.
[101] S. M. Kim, S. J. Ku, G. C. Jo, C. H. Bak, J.-B. Kim, Polymer 2012, 53, 2283.
[102] K. Se Jin, J. Gyeong Cheon, B. Chang Hong, K. Su Min, S. Yu Ri, K. Kwang Ho, K. Se Hun, K. Jin-Baek, Nanotechnology 2013, 24, 085301.
[103] L. T. Schelhas, R. A. Farrell, U. Halim, S. H. Tolbert, Advanced Functional Materials 2014, 24, 6956.
[104] M.-S. She, T.-Y. Lo, H.-Y. Hsueh, R.-M. Ho, NPG Asia Mater 2013, 5, e42.
[105] H.-Y. Hsueh, H.-Y. Chen, M.-S. She, C.-K. Chen, R.-M. Ho, S. Gwo, H. Hasegawa, E. L. Thomas, Nano Letters 2010, 10, 4994.
[106] H.-C. Lee, H.-Y. Hsueh, U. S. Jeng, R.-M. Ho, Macromolecules 2014, 47, 3041.
[107] H.-F. Wang, L.-H. Yu, X.-B. Wang, R.-M. Ho, Macromolecules 2014, 47, 7993.
[108] H.-Y. Hsueh, R.-M. Ho, Langmuir 2012, 28, 8518.
[109] H.-Y. Hsueh, C.-T. Yao, R.-M. Ho, Chemical Society Reviews 2015.
[110] C.-H. Lin, S. Polisetty, L. O'Brien, A. Baruth, M. A. Hillmyer, C. Leighton, W. L. Gladfelter, ACS Nano 2015, 9, 1379.
[111] Q. Peng, Y.-C. Tseng, S. B. Darling, J. W. Elam, Advanced Materials 2010, 22, 5129.
[112] Q. Peng, Y.-C. Tseng, S. B. Darling, J. W. Elam, ACS Nano 2011, 5, 4600.
[113] Y.-C. Tseng, Q. Peng, L. E. Ocola, J. W. Elam, S. B. Darling, The Journal of Physical Chemistry C 2011, 115, 17725.
[114] D. E. Johnston, M. Lu, C. T. Black, MOEMS 2012, 11, 031306.
[115] R. Ruiz, L. Wan, J. Lille, K. C. Patel, E. Dobisz, D. E. Johnston, K. Kisslinger, C. T. Black, Journal of Vacuum Science & Technology B 2012, 30, 06F202.
[116] J. Kamcev, D. S. Germack, D. Nykypanchuk, R. B. Grubbs, C.-Y. Nam, C. T. Black, ACS Nano 2012, 7, 339.
[117] A. Checco, A. Rahman, C. T. Black, Advanced Materials 2014, 26, 886.

[118] A. Checco, B. M. Ocko, A. Rahman, C. T. Black, M. Tasinkevych, A. Giacomello, S. Dietrich, Physical Review Letters 2014, 112, 216101.
[119] A. Rahman, M. Liu, C. T. Black, Journal of Vacuum Science & Technology B 2014, 32.
[120] A. Rahman, C. T. Black, Micro- and Nanotechnology Sensors, Systems, and Applications VI 2014, 9083.
[121] M. Nosonovsky, B. Bhushan, Current Opinion in Colloid & Interface Science 2009, 14, 270.
[122] A. Rahman, A. Ashraf, H. Xin, X. Tong, P. Sutter, M. D. Eisaman, C. T. Black, Nat Commun 2015, 6.
[123] S. B. Darling, N. A. Yufa, A. L. Cisse, S. D. Bader, S. J. Sibener, Advanced Materials 2005, 17, 2446.
[124] S. B. Darling, Surface Science 2007, 601, 2555.
[125] J. G. Son, W. K. Bae, H. Kang, P. F. Nealey, K. Char, ACS Nano 2009, 3, 3927.
[126] T. Ghoshal, T. Maity, J. F. Godsell, S. Roy, M. A. Morris, Advanced Materials 2012, 24, 2390.
[127] T. Ghoshal, R. Senthamaraikannan, M. T. Shaw, J. D. Holmes, M. A. Morris, Nanoscale 2012, 4, 7743.
[128] T. Ghoshal, M. T. Shaw, C. T. Bolger, J. D. Holmes, M. A. Morris, Journal of Materials Chemistry 2012, 22, 12083.
[129] T. Ghoshal, T. Maity, R. Senthamaraikannan, M. T. Shaw, P. Carolan, J. D. Holmes, S. Roy, M. A. Morris, Scientific Reports 2013, 3.
[130] P. Mokarian-Tabari, C. Vallejo-Giraldo, M. Fernandez-Yague, C. Cummins, M. A. Morris, M. J. P. Biggs, Journal of Materials Science-Materials in Medicine 2015, 26.
[131] T. Ghoshal, P. G. Fleming, J. D. Holmes, M. A. Morris, Journal of Materials Chemistry 2012, 22, 22949.
[132] J. Varghese, T. Ghoshal, N. Deepak, C. O'Regan, R. W. Whatmore, M. A. Morris, J. D. Holmes, Chemistry of Materials 2013, 25, 1458.
[133] S. Azlin-Hasim, M. C. Cruz-Romero, T. Ghoshal, M. A. Morris, E. Cummins, J. P. Kerry, Innovative Food Science & Emerging Technologies 2015, 27, 136.
[134] T. Ghoshal, R. Senthamaraikannan, M. T. Shaw, J. D. Holmes, M. A. Morris, Advanced Materials 2014, 26, 1207.
[135] J. Chai, D. Wang, X. Fan, J. M. Buriak, Nature Nanotechnology 2007, 2, 500.
[136] J. Chai, J. M. Buriak, ACS Nano 2008, 2, 489.
[137] N. L. Y. Wu, X. Zhang, J. N. Murphy, J. Chai, K. D. Harris, J. M. Buriak, Nano Letters 2012, 12, 264.
[138] C. Cummins, D. Borah, S. Rasappa, A. Chaudhari, T. Ghoshal, B. M. D. O'Driscoll, P. Carolan, N. Petkov, J. D. Holmes, M. A. Morris, Journal of Materials Chemistry C 2013, 1, 7941.
[139] C. Cummins, A. Gangnaik, R. A. Kelly, D. Borah, J. O'Connell, N. Petkov, Y. M. Georgiev, J. D. Holmes, M. A. Morris, Nanoscale 2015, 7, 6712.
[140] C. Cummins, R. A. Kelly, A. Gangnaik, Y. M. Georgiev, N. Petkov, J. D. Holmes, M. A. Morris, Macromolecular Rapid Communications 2015, 36, 762.
[141] C. Cummins, A. Gangnaik, R. A. Kelly, A. J. Hydes, J. O'Connell, N. Petkov, Y. M. Georgiev, D. Borah, J. D. Holmes, M. A. Morris, Chemistry of Materials 2015, 27, 6091.
[142] S. Park, B. Kim, J. Y. Wang, T. P. Russell, Advanced Materials 2008, 20, 681.
[143] D. O. Shin, D. H. Lee, H. S. Moon, S. J. Jeong, J. Y. Kim, J. H. Mun, H. Cho, S. Park, S. O. Kim, Advanced Functional Materials 2011, 21, 250.
[144] D. O. Shin, J. H. Mun, G.-T. Hwang, J. M. Yoon, J. Y. Kim, J. M. Yun, Y.-B. Yang, Y. Oh, J. Y. Lee, J. Shin, K. J. Lee, S. Park, J. U. Kim, S. O. Kim, ACS Nano 2013, 7, 8899.
[145] J. H. Mun, Y. H. Chang, D. O. Shin, J. M. Yoon, D. S. Choi, K.-M. Lee, J. Y. Kim, S. K. Cha, J. Y. Lee, J.-R. Jeong, Y.-H. Kim, S. O. Kim, Nano Letters 2013, 13, 5720.
[146] J. H. Mun, S. K. Cha, H. Kim, H.-S. Moon, J. Y. Kim, H. M. Jin, Y. J. Choi, J. E. Baek, J. Shin, S. O. Kim, Small 2014, 10, 3742.
[147] W. I. Park, S. Tong, Y. Liu, I. W. Jung, A. Roelofs, S. Hong, Nanoscale 2014, 6, 15216.

[148] M. Biswas, J. A. Libera, S. B. Darling, J. W. Elam, Chemistry of Materials 2014, 26, 6135.
[149] M. Biswas, J. A. Libera, S. B. Darling, J. W. Elam, The Journal of Physical Chemistry C 2015.
[150] Y.-C. Tseng, Q. Peng, L. E. Ocola, D. A. Czaplewski, J. W. Elam, S. B. Darling, Journal of Materials Chemistry 2011, 21, 11722.
[151] Y.-C. Tseng, Q. Peng, L. E. Ocola, D. A. Czaplewski, J. W. Elam, S. B. Darling, Journal of Vacuum Science & Technology B 2011, 29, 06FG01.
[152] Y.-C. Tseng, A. U. Mane, J. W. Elam, S. B. Darling, Advanced Materials 2012, 24, 2608.
[153] H. Cho, H. Park, S. Park, H. Choi, H. Huang, T. Chang, Journal of Colloid and Interface Science 2011, 356, 1.
[154] T. Lohmüller, D. Aydin, M. Schwieder, C. Morhard, I. Louban, C. Pacholski, J. Spatz, Biointerphases 2011, 6, MR1.
[155] H. Cho, H. Park, T. P. Russell, S. Park, Journal of Materials Chemistry 2010, 20, 5047.
[156] M. Roulet, M. Vayer, C. Sinturel, European Polymer Journal 2013, 49, 3897.
[157] S. Biswas, J. Doherty, D. Majumdar, T. Ghoshal, K. Rahme, M. Conroy, A. Singha, M. A. Morris, J. D. Holmes, Chemistry of Materials 2015, 27, 3408.
[158] A. Chaudhari, T. Ghoshal, M. T. Shaw, C. Cummins, D. Borah, J. D. Holmes, M. A. Morris, "Formation of sub-7 nm feature size PS-b-P4VP block copolymer structures by solvent vapour process", 2014.
[159] O. Lotty, S. Biswas, T. Ghoshal, C. Glynn, C. O' Dwyer, N. Petkov, M. A. Morris, J. D. Holmes, Journal of Materials Chemistry C 2013, 1, 4450.
[160] S. Rasappa, T. Ghoshal, D. Borah, R. Senthamaraikannan, J. D. Holmes, M. A. Morris, Scientific Reports 2015, 5, 13270.
[161] J. Li, T. Zhao, T. Chen, Y. Liu, C. N. Ong, J. Xie, Nanoscale 2015.
[162] P. K. Jain, X. Huang, I. H. El-Sayed, M. A. El-Sayed, Accounts of Chemical Research 2008, 41, 1578.
[163] E. B. Gowd, B. Nandan, M. K. Vyas, N. C. Bigall, A. Eychmueller, H. Schloerb, M. Stamm, Nanotechnology 2009, 20.
[164] B. Nandan, E. B. Gowd, N. C. Bigall, A. Eychmüller, P. Formanek, P. Simon, M. Stamm, Advanced Functional Materials 2009, 19, 2805.
[165] N. C. Bigall, B. Nandan, E. B. Gowd, A. Horechyy, A. Eychmüller, ACS Applied Materials & Interfaces 2015, 7, 12559.
[166] M. K. Mayeda, J. Hayat, T. H. Epps, J. Lauterbach, Journal of Materials Chemistry A 2015, 3, 7822.
[167] C. M. Fernyhough, D. Pantazis, S. Pispas, N. Hadjichristidis, European Polymer Journal 2004, 40, 237.
[168] U. Nagpal, F. A. Detcheverry, P. F. Nealey, J. J. de Pablo, Macromolecules 2011, 44, 5490.
[169] N. Hadjichristidis, H. Iatrou, M. Pitsikalis, S. Pispas, A. Avgeropoulos, Progress in Polymer Science 2005, 30, 725.
[170] N. Hadjichristidis, A. Hirao, Y. Tezuka, F. DuPrez, *Complex Macromolecular Architectures: Synthesis, Characterization, and Self-Assembly*, Wiley, 2011.
[171] C. A. Ross, Y. S. Jung, V. P. Chuang, J. G. Son, K. W. Gotrik, R. A. Mickiewicz, J. K. W. Yang, J. B. Chang, K. K. Berggren, J. Gwyther, I. Manners, "Templated self-assembly of Si-containing block copolymers for nanoscale device fabrication", presented at *Proceedings of SPIE - The International Society for Optical Engineering*, 2010.
[172] F. S. Bates, G. H. Fredrickson, Physics Today 1999, 52, 32.
[173] W. Zheng, Z.-G. Wang, Macromolecules 1995, 28, 7215.
[174] M. E. Davis, Nature 2002, 417, 813.
[175] J. S. Beck, J. C. Vartuli, W. J. Roth, M. E. Leonowicz, C. T. Kresge, K. D. Schmitt, C. T. W. Chu, D. H. Olson, E. W. Sheppard, Journal of the American Chemical Society 1992, 114, 10834.
[176] R. A. Farrell, N. Petkov, M. A. Morris, J. D. Holmes, Journal of Colloid and Interface Science 2010, 349, 449.

[177] P. Yang, D. Zhao, B. F. Chmelka, G. D. Stucky, Chemistry of Materials 1998, 10, 2033.
[178] D. Zhao, Q. Huo, J. Feng, B. F. Chmelka, G. D. Stucky, Journal of the American Chemical Society 1998, 120, 6024.
[179] P. Yang, D. Zhao, D. I. Margolese, B. F. Chmelka, G. D. Stucky, Nature 1998, 396, 152.
[180] P. D. Yang, T. Deng, D. Y. Zhao, P. Y. Feng, D. Pine, B. F. Chmelka, G. M. Whitesides, G. D. Stucky, Science 1998, 282, 2244.
[181] A. V. Kabanov, P. Lemieux, S. Vinogradov, V. Alakhov, Advanced Drug Delivery Reviews 2002, 54, 223.
[182] S. Fusco, A. Borzacchiello, P. A. Netti, Journal of Bioactive and Compatible Polymers 2006, 21, 149.
[183] E. V. Batrakova, A. V. Kabanov, Journal of Controlled Release 2008, 130, 98.
[184] A. Pitto-Barry, N. P. E. Barry, Polymer Chemistry 2014, 5, 3291.
[185] L. E. Bromberg, E. S. Ron, Advanced Drug Delivery Reviews 1998, 31, 197.
[186] M. C. Orilall, U. Wiesner, Chemical Society Reviews 2011, 40, 520.
[187] M. Stefik, S. Guldin, S. Vignolini, U. Wiesner, U. Steiner, Chemical Society Reviews 2015.
[188] J. Kao, K. Thorkelsson, P. Bai, B. J. Rancatore, T. Xu, Chemical Society Reviews 2013, 42, 2654.
[189] K. Thorkelsson, P. Bai, T. Xu, Nano Today 2015, 10, 48.
[190] S. Ludwigs, A. Boker, A. Voronov, N. Rehse, R. Magerle, G. Krausch, Nat Mater 2003, 2, 744.
[191] I. A. Zucchi, E. Poliani, M. Perego, Nanotechnology 2010, 21.
[192] D. Borah, S. Rasappa, R. Senthamaraikannan, J. D. Holmes, M. A. Morris, Langmuir 2013, 29, 8959.
[193] M. Aizawa, J. M. Buriak, Journal of the American Chemical Society 2006, 128, 5877.
[194] J. Bang, S. H. Kim, E. Drockenmuller, M. J. Misner, T. P. Russell, C. J. Hawker, Journal of the American Chemical Society 2006, 128, 7622.
[195] D. H. Lee, S. Park, W. Gu, T. P. Russell, ACS Nano 2011, 5, 1207.
[196] J. N. L. Albert, W.-S. Young, R. L. Lewis, T. D. Bogart, J. R. Smith, T. H. Epps, ACS Nano 2011, 6, 459.
[197] M. S. Tureau, T. H. Epps, Macromolecules 2012, 45, 8347.
[198] M. K. Mayeda, W.-F. Kuan, W.-S. Young, J. A. Lauterbach, T. H. Epps, Chemistry of Materials 2012, 24, 2627.
[199] F. S. Bates, M. A. Hillmyer, T. P. Lodge, C. M. Bates, K. T. Delaney, G. H. Fredrickson, Science 2012, 336, 434.
[200] M. D. Rodwogin, C. S. Spanjers, C. Leighton, M. A. Hillmyer, ACS Nano 2010, 4, 725.
[201] T. Kubo, R. F. Wang, D. A. Olson, M. Rodwogin, M. A. Hillmyer, C. Leighton, Applied Physics Letters 2008, 93.
[202] S. E. Querelle, E. A. Jackson, E. L. Cussler, M. A. Hillmyer, ACS Applied Materials & Interfaces 2013, 5, 5044.
[203] L. M. Pitet, M. A. Amendt, M. A. Hillmyer, Journal of the American Chemical Society 2010, 132, 8230.
[204] J. Rzayev, M. A. Hillmyer, Journal of the American Chemical Society 2005, 127, 13373.
[205] V. P. Chuang, C. A. Ross, J. Gwyther, I. Manners, Advanced Materials 2009, 21, 3789.
[206] H. K. Choi, N. M. Aimon, D. H. Kim, X. Y. Sun, J. Gwyther, I. Manners, C. A. Ross, ACS Nano 2014, 8, 9248.
[207] H. K. Choi, J. Gwyther, I. Manners, C. A. Ross, ACS Nano 2012, 6, 8342.
[208] K. Aissou, H. K. Choi, A. Nunns, I. Manners, C. A. Ross, Nano Letters 2013, 13, 835.
[209] K. Aissou, A. Nunns, I. Manners, C. A. Ross, Small 2013, 9, 4077.
[210] A. N. Semenov, Macromolecules 1993, 26, 6617.
[211] R. L. Bristol, in *Advances in Resist Materials and Processing Technology XXIV*, Vol. 6519 (Ed: Q. Lin), 2007, W5190.
[212] D. J. C. Herr, Journal of Materials Research 2011, 26, 122.

[213] S. H. Kim, M. J. Misner, L. Yang, O. Gang, B. M. Ocko, T. P. Russell, Macromolecules 2006, 39, 8473.
[214] A. A. Teran, N. P. Balsara, The Journal of Physical Chemistry B 2014, 118, 4.
[215] T. Ghoshal, C. Ntaras, M. T. Shaw, J. D. Holmes, A. Avgeropoulos, M. A. Morris, Journal of Materials Chemistry C 2015.
[216] Z. Sun, Z. Chen, W. Zhang, J. Choi, C. Huang, G. Jeong, E. B. Coughlin, Y. Hsu, X. Yang, K. Y. Lee, D. S. Kuo, S. Xiao, T. P. Russell, Advanced Materials 2015.
[217] J. D. Cushen, I. Otsuka, C. M. Bates, S. Halila, S. Fort, C. Rochas, J. A. Easley, E. L. Rausch, A. Thio, R. Borsali, C. G. Willson, C. J. Ellison, ACS Nano 2012, 6, 3424.
[218] I. Otsuka, T. Isono, C. Rochas, S. Halila, S. Fort, T. Satoh, T. Kakuchi, R. Borsali, ACS Macro Letters 2012, 1, 1379.
[219] I. Otsuka, S. Tallegas, Y. Sakai, C. Rochas, S. Halila, S. Fort, A. Bsiesy, T. Baron, R. Borsali, Nanoscale 2013, 5, 2637.
[220] B. R. Sveinbjoernsson, R. A. Weitekamp, G. M. Miyake, Y. Xia, H. A. Atwater, R. H. Grubbs, Proceedings of the National Academy of Sciences of the United States of America 2012, 109, 14332.
[221] E. Kim, H. Ahn, S. Park, H. Lee, M. Lee, S. Lee, T. Kim, E.-A. Kwak, J. H. Lee, X. Lei, J. Huh, J. Bang, B. Lee, D. Y. Ryu, ACS Nano 2013, 7, 1952.
[222] S. W. Hong, W. Gu, J. Huh, B. R. Sveinbjornsson, G. Jeong, R. H. Grubbs, T. P. Russell, ACS Nano 2013, 7, 9684.
[223] Y. Xia, B. D. Olsen, J. A. Kornfield, R. H. Grubbs, Journal of the American Chemical Society 2009, 131, 18525.
[224] K. Koo, H. Ahn, S.-W. Kim, D. Y. Ryu, T. P. Russell, Soft Matter 2013, 9, 9059.
[225] D. Borah, T. Ghoshal, M. T. Shaw, A. Chaudhari, N. Petkov, A. P. Bell, J. D. Holmes, M. A. Morris, Nanomaterials and Nanotechnology 2014, 4.
[226] D. F. Sunday, M. R. Hammond, C. Wang, W.-l. Wu, R. J. Kline, G. E. Stein, Journal of Micro-Nanolithography Mems and Moems 2013, 12.
[227] D. F. Sunday, M. R. Hammond, C. Wang, W.-l. Wu, D. M. Delongchamp, M. Tjio, J. Y. Cheng, J. W. Pitera, R. J. Kline, ACS Nano 2014, 8, 8426.
[228] D. F. Sunday, E. Ashley, L. Wan, K. C. Patel, R. Ruiz, R. J. Kline, Journal of Polymer Science Part B-Polymer Physics 2015, 53, 595.
[229] T. Segal-Peretz, J. Winterstein, M. Doxastakis, A. Ramírez-Hernández, M. Biswas, J. Ren, H. S. Suh, S. B. Darling, J. A. Liddle, J. W. Elam, J. J. de Pablo, N. J. Zaluzec, P. F. Nealey, ACS Nano 2015, 9, 5333.
[230] K. W. Gotrik, T. Lam, A. F. Hannon, W. Bai, Y. Ding, J. Winterstein, A. Alexander-Katz, J. A. Liddle, C. A. Ross, Advanced Functional Materials 2014, 24, 7689.
[231] H. G. Yoo, M. Byun, C. K. Jeong, K. J. Lee, Advanced Materials 2015.
[232] P. W. Majewski, A. Rahman, C. T. Black, K. G. Yager, Nat Commun 2015, 6.
[233] S. Y. Kim, A. Nunns, J. Gwyther, R. L. Davis, I. Manners, P. M. Chaikin, R. A. Register, Nano Letters 2014, 14, 5698.
[234] W. I. Park, Y. Kim, J. W. Jeong, K. Kim, J.-K. Yoo, Y. H. Hur, J. M. Kim, E. L. Thomas, A. Alexander-Katz, Y. S. Jung, Scientific Reports 2013, 3, 3190.
[235] W. I. Park, J. M. Kim, J. W. Jeong, Y. H. Hur, Y. J. Choi, S.-H. Kwon, S. Hong, Y. Yin, Y. S. Jung, K. H. Kim, Chemistry of Materials 2015, 27, 2673.
[236] P. A. R. Delgadillo, R. Gronheid, C. J. Thode, H. Wu, Y. Cao, M. Neisser, M. Somervell, K. Nafus, P. F. Nealey, MOEMS 2012, 11, 031302.
[237] C.-C. Liu, I. C. Estrada-Raygoza, J. Abdallah, S. Holmes, Y. Yin, A. Schepis, M. Cicoria, D. Hetzer, H. Tsai, M. Guillorn, M. Tjio, J. Cheng, M. Somervell, M. Colburn, "Directed self-assembly process implementation in a 300mm pilot line environment", 2013.
[238] S. Isabelle, T. Raluca, G. Ahmed, A. Maxime, J. Karine, C.-M. Gaëlle, B. Patricia Pimenta, C. Xavier, B. Jérôme, B. Xavier, M. Sylvain, N. Christophe, C. Gilles, B. Sébastien, A. Masaya, P. Charles, Japanese Journal of Applied Physics 2014, 53, 06JC05.

[239] G. Rhys Alun, W. Aled, O. Chloe, R. Jonathan, V. Aravind, T. Thomas, Journal of Physics D: Applied Physics 2013, 46, 503001.
[240] L. Wan, R. Ruiz, H. Gao, K. C. Patel, J. Lille, G. Zeltzer, E. A. Dobisz, A. Bogdanov, P. F. Nealey, T. R. Albrecht, MOEMS 2012, 11, 031405.
[241] X. Zhang, J. N. Murphy, N. L. Y. Wu, K. D. Harris, J. M. Buriak, Macromolecules 2011, 44, 9752.
[242] D. Borah, M. T. Shaw, J. D. Holmes, M. A. Morris, ACS Applied Materials & Interfaces 2013, 5, 2004.
[243] D. Borah, R. Senthamaraikannan, S. Rasappa, B. Kosmala, J. D. Holmes, M. A. Morris, ACS Nano 2013, 7, 6583.
[244] P. Mokarian-Tabari, C. Cummins, S. Rasappa, C. Simao, C. M. Sotomayor Torres, J. D. Holmes, M. A. Morris, Langmuir 2014, 30, 10728.
[245] S. Rasappa, L. Schulte, D. Borah, M. A. Morris, S. Ndoni, Colloids and Interface Science Communications 2014, 2, 1.
[246] A. G. Jacobs, B. Jung, C. K. Ober, M. O. Thompson, "Control of PS-*b*-PMMA directed self-assembly registration by laser induced millisecond thermal annealing", 2014.
[247] P. W. Majewski, K. G. Yager, ACS Nano 2015, 9, 3896.

Table of contents (TOC) Graphic:

